Title

The System for Classification of Low-Pressure Systems (SyCLoPS): An All-In-One Objective Framework for Large-Scale Data Sets

Journal

Journal of Geophysical Research: Atmospheres, 130(1)

ISSN

2169-897X

Authors

Han, Yushan

Ullrich, Paul A

Publication Date

2025-01-16

DOI

10.1029/2024jd041287

JGR Atmospheres

RESEARCH ARTICLE
10.1029/2024JD041287

The System for Classification of Low-Pressure Systems (SyCLoPS): An All-In-One Objective Framework for Large-Scale Data Sets

Yushan Han[1] **and Paul A. Ullrich**[1,2]

[1]Department of Land, Air and Water Resources, University of California, Davis, Davis, CA, USA, [2]Division of Physical and Life Sciences, Lawrence Livermore National Laboratory, Livermore, CA, USA

Key Points:

- The first all-inclusive low-pressure system (LPS) detection and classification framework for climate data and model outputs is proposed
- The framework substantially extends LPS track lengths while improving tropical cyclone detection skill
- The framework is useful to study the frequency, structure, development, wind impact, and precipitation contribution of each type of LPS

Supporting Information:

Supporting Information may be found in the online version of this article.

Correspondence to:

Y. Han,
yshhan@ucdavis.edu

Citation:

Han, Y., & Ullrich, P. A. (2025). The system for classification of low-pressure systems (SyCLoPS): An all-in-one objective framework for large-scale data sets. *Journal of Geophysical Research: Atmospheres*, *130*, e2024JD041287. https://doi.org/10.1029/2024JD041287

Received 2 APR 2024
Accepted 16 DEC 2024

Abstract We propose the first unified objective framework (SyCLoPS) for detecting and classifying all types of low-pressure systems (LPSs) in a given data set. We use the state-of-the-art automated feature tracking software TempestExtremes (TE) to detect and track LPS features globally in ERA5 and compute 16 parameters from commonly found atmospheric variables for classification. A Python classifier is implemented to classify all LPSs at once. The framework assigns 16 different labels (classes) to each LPS data point and designates four different types of high-impact LPS tracks, including tracks of tropical cyclone (TC), monsoonal system, subtropical storm and polar low. The classification process involves disentangling high-altitude and drier LPSs, differentiating tropical and non-tropical LPSs using novel criteria, and optimizing for the detection of the four types of high-impact LPS. A comparison of our labels with those in the International Best Track Archive for Climate Stewardship (IBTrACS) revealed an overall accuracy of 95% in distinguishing between tropical systems, extratropical cyclones, and disturbances. SyCLoPS produces a better TC detection skill compared to the previous algorithms, highlighted by an approximately 6% reduction in the false alarm rate compared to the previous TE algorithm. The vertical cross section composite of the four types of high-impact LPS we detect each shows distinct structural characteristics. Finally, we demonstrate that SyCLoPS is valuable for investigating various aspects of LPSs in climate data, such as the evolution of a single LPS track, patterns of LPS frequencies, and precipitation or wind influence associated with a particular LPS class.

Plain Language Summary We create a new objective framework (SyCLoPS) that can detect, track, and categorize different kinds of cyclones (low-pressure systems) in data sets. We use an advanced software called TempestExtremes to spot cyclones globally in ERA5 reanalysis and then use a Python program to sort all cyclones into 16 different groups based on their characteristics. We also identify four types of significant cyclone tracks: tracks of tropical cyclones, monsoonal systems, subtropical storms, and polar lows. The framework can recognize cyclones over high-elevation areas and dry cyclones. It can also efficiently separate tropical low-pressure systems and extratropical (non-tropical) systems using a novel method. We compare our results against existing catalogs and find that the framework produces objectively tracked tropical cyclones that better match the observations, and the labels given by the framework are in good agreement with those given in the subjective catalogs. We also show the distinct vertical structures for the four types of significant cyclones we identify. Finally, we demonstrate that SyCLoPS can help us understand various aspects of low-pressure systems in climate data, like how they evolve over time, where they occur more frequently, and their related extreme weather.

1. Introduction

In response to the growing need for advanced impacts-relevant model and climate data analysis, objective feature detection has emerged as a key tool for detecting and tracking various meteorological features in large-scale data sets. Researchers give considerable attention to detecting and tracking low-pressure systems (LPSs), or cyclones, which are often drivers for high-impact weather including high winds and extreme precipitation. Some more significant LPSs, such as tropical cyclones (TCs), monsoon lows (MLs) or monsoon depressions (MDs), subtropical cyclones (SCs), and extratropical cyclones (EXs), are commonly tracked using specialized tracking algorithms in reanalysis and climate model outputs to derive their climatology and perform climate projections (e.g., Guishard et al., 2009; Hurley & Boos, 2015; Neu et al., 2013; Roberts et al., 2020a, 2020b). Tropical-like cyclones (TLCs) refer to those storms in the subtropics and the polar regions that share many similarities with

TCs, including Mediterranean hurricanes and polar lows (PLs). They are capable of producing significant coastal hazards (Toomey et al., 2022), but more rigorous automated tracking has only occurred relatively recently because of advances in model resolution and observations (e.g., Flaounas et al., 2023; Stoll, 2022; Stoll et al., 2018; Zhang et al., 2021).

TempestExtremes (TE; Ullrich & Zarzycki, 2017; Ullrich et al., 2021) is an all-inclusive, state-of-the-art automated Lagrangian feature tracking software package. It is designed to robustly and efficiently detect, track, and analyze any nodal or areal features in large-scale data sets with user-friendly command lines and using parallelized C++. TE has been optimized for TC detection using geopotential thickness and mean sea level pressure (MSLP) closed contour criteria (Zarzycki & Ullrich, 2017). Bourdin et al. (2022) found that TC detection using TE outperforms other methods for the reanalysis data set ERA5 (Hersbach et al., 2020). Vishnu et al. (2020) used TE to track monsoonal systems (MSs), which includes MLs and MDs, in the North Indian Ocean across different reanalysis products, and observed high success rates. TE's detector has also been combined with the cyclone phase space (CPS) of Hart (2003), which classifies storms based on thermal wind and thermal asymmetry parameters. For example, Zarzycki et al. (2017) used TE and CPS to track both TCs and post-TCs/EXs based on LPSs' thermal structure, and detect extratropical transition. Zhang et al. (2021) used a similar approach to detect Mediterranean hurricanes.

Although TE's algorithms are powerful for LPS detection, when applied standalone it generally needs to adopt strict criteria to avoid mischaracterizing features. Unfortunately, this issue is unavoidable when using any specialized method, and controls like seasonality, topographical masks, and latitudinal bounds are required to avoid polluting the data set with incorrect detections (i.e., false alarms). For example, TE's TC detection algorithm enforces a 50° highest latitude and a 150 $m^2 s^{-2}$ highest surface geopotential limit on detected LPS tracks. Another popular TC track algorithm TRACK requires TC tracks to start between 30°S and 30°N (K. Hodges et al., 2017). Vishnu et al. (2020) tracked MSs only between June and September and in parts of the North Indian Ocean, further requiring detected LPSs to maintain at least 24 hr offshore. Stoll (2022) tracked PLs by first excluding tracks outside of the 30–80° band of both hemispheres and excluding features over defined open water regions. Since the aforementioned algorithms are all designed for single-type LPS detection, they also need to filter other types of LPS tracks or other types of LPS nodes (data points) in a detected track that don't meet the specified criteria and thresholds. With these limitations, features tracked by the existing algorithms often end or break abruptly and are shorter in length than analogs in manually tracked data sets. Consequently, information from the complete LPS lifespan is not available. While the CPS approach can classify the thermal structure evolution of an LPS throughout its lifetime, it is not designed for broader LPS classification, as different types of LPS often share similar thermal structures. For example, mature TCs, some post-TCs, EXs experiencing warm seclusion and some subtropical or hybrid cyclones can all be categorized as shallow or deep symmetric warm-core systems according to the CPS (Hart, 2003). Conversely, cold-core systems are ubiquitous across latitudes, as evidenced by the prevalence of low-level cold cores in many weak tropical systems (Hopsch et al., 2010; Hunt et al., 2016; Reed et al., 1977). Hence, warm/cold core criteria are likely insufficient to effectively classify global LPSs.

Instead of trying to develop multiple specialized trackers, we propose a new objective framework, called the System for Classification of Low-Pressure Systems (SyCLoPS), to detect, track, and classify all detectable LPSs worldwide at once, without any spatial or seasonal limitations. We test our framework in ERA5, and focus exclusively on surface-level LPSs (so upper-level disturbances and lows are out of our scope). The detection and tracking are completed using TE commands, and the classification is done in a separate Python classifier that assigns 16 different types of LPS labels/classes (TC, ML, EX, SC, PL, etc.) and 4 types of high-impact LPS tracks, which are TC Track, MS Track, and two types of TLC Tracks (subtropical TLC (STLC) and PL tracks). The classification process is based primarily on conventional definitions and physical (dynamical/thermodynamic) nature of different LPSs, and is simplified to the extent possible. The atmospheric variables used for classification are commonly found in reanalysis and climate model outputs and the parameters used to classify LPSs can be directly computed by TE for each detected LPS node. Basic machine learning techniques and mathematical optimization are used to refine our thresholds against archives of observed and subjectively identified LPSs. The resulting framework involves only thresholds on basic meteorological fields and includes no "black box" elements.

Table 1
Initialism Table for Low-Pressure System Types and Detection Skill Metrics

Initialism	Full term	Definition
HAL	High-altitude Low	LPSs found at high altitudes without a warm core
THL	Thermal low	Shallow systems featuring a dry and warm lower core
HATHL	High-altitude Thermal Low	LPSs found at high altitudes with a warm core
DOTHL	Deep (Orographic) Thermal Low	Non-shallow LPSs featuring a dry and warm lower core driven by topography
TC	Tropical Cyclone	LPSs that would be named in IBTrACS
TD	Tropical Depression	Defined in Section 4.2
TLO	Tropical Low	Non-shallow tropical systems that fall short of TD requirements
MD	Monsoon Depression	TDs developing in monsoonal environment. Also denoted as TD(MD)
ML	Monsoon Low	TLOs developing in monsoonal environment. Also denoted as TLO(ML)
MS	Monsoonal System	Monsoon LPSs (MDs plus MLs)
TLC	Tropical-Like Cyclone	Non-tropical LPSs that resemble TCs
SS (STLC)	Subtropical Storm (Subtropical Tropical-Like Cyclone)	Type of TLC. Defined in Section 2
PL (PTLC)	Polar Low (Polar Tropical-Like Cyclone)	Type of TLC. Defined in Section 2
SC	Subtropical Cyclone	Defined in Section 4.3
EX	Extratropical Cyclone	Most typical non-tropical cyclones
DS	Disturbance	Shallow LPSs or waves with weak surface circulations. DSD, DST and DSE are dry, tropical and extratropical DSs
QS	Quasi-stationary	LPSs that stay relatively localized
HR/FAR/IR	Hit Rate/False Alarm Rate/Infrequency Rate	Defined in Sections 5.1 and 5.3
HRMFAR	Hit Rate Minus False Alarm Rate	TC detection skill metric. See Section 5.1
CSI	Critical Success Index	MS detection skill metric. See Section 5.2
HRMIR	Hit Rate Minus Infrequency Rate	TLC detection skill metric. See Section 5.3

The new framework produces considerably longer LPS tracks because of the low detection threshold we choose. The labeled LPS nodes are also directly comparable to the subjective LPS status (labels) in the International Best Track Archive for Climate Stewardship (IBTrACS) (Knapp et al., 2010). Labeled tracks are also comparable to other subjective TC, MS, and TLC track catalogs. When compared to these catalogs, the framework maintains or improves on the LPS detection skill of the specialized trackers (under a variety of metrics) without implementation of the aforementioned restrictions. For example, other TC detection frameworks will often pick up some stronger warm-core extratropical or subtropical systems that were not recorded in IBTrACS even if latitudinal bounds were enforced (Bourdin et al., 2022). The new algorithm addresses this problem, leading to a noticeable increase in TC detection skill without further post-processing.

The manuscript is structured as follows. Section 2 summarizes all the data sets we use to verify our classification thresholds and quantify LPS detection skill. Sections 3–5 explain the general detection and classification processes and justify each of the conditions we set for classification. In Section 6, we include some highlights from the classified LPS catalog and discuss potential applications of the SyCLoPS framework. Section 7 concludes the paper and addresses known limitations. For the readers' convenience, Table 1 summarized all the initialisms and definitions of LPS types (classes) and detection skill metrics we use in this article.

2. Data

We detect, track, and classify LPSs from 1979 to 2022 in ERA5 at 3-hourly frequency. ERA5 is used for developing SyCLoPS since we include detection of small or mesoscale features like early-stage TCs and TLCs, which require reanalysis with finer data resolution. Although SyCLoPS is developed using ERA5, it uses a small number of commonly output meteorological fields and so is intended to be applicable to other global or regional meteorological data sets. A list of ERA5 variables used in SyCLoPS is given in Appendix A. Since climate model data often have a different format and frequency, and may be missing some of the ERA5 variables used to develop

SyCLoPS, we perform adaptation experiments on SyCLoPS using alternative ERA5 fields to demonstrate how SyCLoPS could be adapted to climate model outputs (Appendix B). The results show that SyCLoPS can be slightly modified to adapt to a variety of data formats while maintaining good performance.

By design, SyCLoPS uses TE's closed contour criteria to compute many of its classification parameters since the closed contour criteria is largely insensitive to model resolution (Ullrich & Zarzycki, 2017). TE's closed contour criteria uses graph search to ensure that all paths along the unstructured grid from a field's local maximum (or minimum) decrease (or increase) before reaching a specified great-circle distance (GCD). For example, a positive closed contour in MSLP with delta MSLP (ΔMSLP) uses graph search to ensure that all paths along the unstructured grid from a local minimum ($MSLP_0$) pass through a node with value greater than or equal to $MSLP_0 + \Delta MSLP$ before reaching the specified GCD.

Four types of high-impact LPS we detect, which includes TCs, MSs and two types of TLCs, are verified against four subjective data sets to evaluate detection skill. TCs are verified against the widely used IBTrACS data set. Specifically, we verify against 3510 main-type tracks from 1979 to 2021 inclusive that meet the minimum requirement for a TC to be considered formed and named by global agencies—with peak wind speeds of at least 34 knots (17.5 m s^{-1}). Hence, TC detection in SyCLoPS follows the same definition as the agencies. We refer to this subset of IBTrACS as IB-TC. For MSs, we use the Sikka archive Sikka (2006) for verification, which provides manually-identified North Indian Ocean monsoonal system positions on historic surface weather maps at daily frequency, digitized by Hurley and Boos (2015).

In SyCLoPS, we regard subtropical storms (SSs) and polar lows (PLs) as TLCs that develop in the subtropics and the polar regions. Hence, they can also be denoted as STLCs and polar TLCs (PTLCs). Few subjective data sets are available for these two types of TLCs. SSs are regarded as the more intense subtropical or hybrid cyclones that carry at least gale-force surface sustained winds (Guishard et al., 2009; National Hurricane Center, n.d.). Mediterranean TLCs (hurricanes) may be viewed as being among global SSs, and they are perhaps most well studied, with relatively more observational data available. However, existing subjective data sets for those storms are still very incomplete. To reconstruct a more credible subjective archive for Mediterranean TLCs (representing SSs), we obtain the subjectively tracked data from Flaounas et al. (2023), wherein trained meteorologists identify and track Mediterranean cyclones, including TLCs and other noticeable systems in the region, using ERA5's MSLP field. We then use the cyclone information table provided in Flaounas et al. (2023) and two online sources (see Data Availability Statement section) to select tracks that can be potentially classified as SSs (as defined above), while avoiding weaker systems. We also observe that IBTrACS contains a few subtropical storm records, which agencies tend to record when they have the potential to transform into TCs. However, these records are largely incomplete and can often be confused with weaker TCs, so we do not separate them from the TC archive and include them in the SS archive.

We verify PL detection against the well-known and widely-used STARS (sea surface temperature (SST) and Altimeter Synergy for Improved Forecasting of Polar Lows) data set (Noer et al., 2011). This subjective PL data set is constructed based on the frequently cited PL definition from Rasmussen and Turner (2003)—"A polar low is a small, but fairly intense maritime cyclone that forms poleward of the main baroclinic zone (the polar front or other major baroclinic zone). The horizontal scale of the polar low is approximately between 200 and 1,000 km and surface winds near or above gale force." STARS contains 185 polar lows subjectively identified by the Norwegian Meteorological Institute from 2002 to 2011 in parts of the Nordic Seas, based on synoptic-scale analysis in their weather model and satellite infrared data. There exists other less popular subjective PL data sets that record substantially more PLs, including many LPS sub-centers in multi-center PL cases, found in the same region using different satellite data (Stoll, 2022). This implies there is ambiguity in the PL definition, likely aggravated by a lack of near-surface observations for accurate evaluations. It should also be noted that a model/data resolution as coarse as ERA5 may simply be incapable of "seeing" some small or multi-centered TLC cases, regardless of the detection criteria applied. For example, Stoll (2022) reported that only 61%–81% of PLs in the existing PL data sets have a matched LPS track in ERA5.

In our objectively tracked LPS data set, we match our tracks to the tracks in each subjective data set using different matching algorithms, describedText S1 in Supporting Information S1. To avoid misclassification of MSs, we also use an objectively tracked North Atlantic easterly wave (EW) data set (Lawton et al., 2022) to construct a

corresponding surface LPS data set (also see Text S1 in Supporting Information S1). These matched TC, MS, SS, PL, and EW data sets are later used in the classification and data analysis process.

3. The Overall Workflow

MSLP is the starting point for our LPS node detection. Although prior research has also employed 850 hPa vorticity or streamfunction fields to detect monsoon LPSs and other cyclones (e.g., K. I. Hodges, 1994; Hurley & Boos, 2015; Vishnu et al., 2020), we consider MSLP a preferable variable for two reasons: (a) local minima/maxima of MSLP are widely used in meteorological agency operations to locate surface pressure systems, including LPSs in IBTrACS; and (b) there is a global agency consensus on the definition of MSLP (Knapp et al., 2010). Further, low-level vorticity or streamfunction data may not be directly available in many data sets when intersecting with the surface, and they have opposite signs for cyclonic systems in the Northern and Southern Hemispheres, which could lead to tracks across equatorial regions becoming disconnected if they are not detected and tracked twice using different signs. These factors all contribute to the computational burden of detecting LPSs globally without spatial limitations.

MSLP signals may be generally weaker in the tropics, which makes it difficult to differentiate some weaker LPSs associated with tropical waves. To capture these features in the tracker, we have aimed for the lowest reasonable detection threshold. With this in mind, an LPS node (center) is flagged at a local minimum MSLP if the MSLP value is lower than its surrounding by at least 10 Pa (0.1 hPa) within 5.5° GCD from the node (a 10-Pa delta positive closed contour criterion). Although we find this is an extremely low threshold, very weak EWs (particularly those over land) that don't have the minimal surface closed MSLP contour will not be detected.

The first step taken by TE is pointwise detection of LPS nodes. Besides the MSLP closed contour criterion, we also require that nodal candidates located within 6° GCD of each other merge into a single node, preserving the one with the lowest MSLP value, which aligns with the specification in Zarzycki and Ullrich (2017). The second step in TE connects consecutive nodes in time and form LPS tracks, which requires tuning argument specifications in TE to meet the following criteria:

1. LPSs must at least sustain for a time span of 18 hr to avoid too many weak, short-lived, diurnal lows.
2. Nodal candidates in two consecutive time steps must be located within 4° GCD distance of each other. This specification is chosen based on the fact that the translation speed of the fastest EXs rarely go over 40 m s^{-1}, or about 140 km per hour (Bernhardt & DeGaetano, 2012; Lodise et al., 2022).
3. A maximum allowable gap of 12 hr within a track is implemented. A longer gap time is not preferred because it may include too many weak diurnal lows.
4. To exclude negligible LPSs, a track must contain at least 5 time steps during which the MSLP at the LPS node is 100 Pa lower than its surrounding (within a 5.5° GCD from the node).

A total of 7,781,105 data points (nodes) and 379,301 distinct tracks are identified in the 44-year period from 1979 to 2022. The whole tracking process takes about 2 hr using 2 NERSC Perlmutter nodes (each with 128 threads). During the first two steps, TE also conveniently computes 15 parameters (data columns) from input variable fields and outputs them to each node in the detected LPS tracks. In the third step of TE, we prepare the data for computing the LPS size parameter (LPSAREA) by running additional TE commands. After completing TE procedures, a Python classifier script is implemented to first compute LPSAREA and form the input (LPS) catalog for classification, structured in accordance with our catalog column table in Appendix C. The input catalog includes a list of 16 parameters that are used throughout the classification process explained below. The Python classifier then classifies each LPS node based on conditions on those input parameters and assigns them labels from the 16 distinct classes, following the workflow illustrated in the accompanying flowchart (Figure 1). We call the output of this classification workflow the classified (LPS) catalog. The structure of this catalog can also be found in Appendix C. Please refer to Text S5 in Supporting Information S1 for a brief explanation for the selection of the specifications in the parameters used in the input catalog. TE commands used to implement the framework are printed Text S6 in Supporting Information S1. The required TE and Python script files, both LPS catalogs, and a manual for using SyCLoPS data are all uploaded to Zenodo (see Data Availability Statement section).

Most of the criteria chosen for classification of these systems are largely insensitive to climate change because they are based on conventional definitions (the nature of LPSs) and subjective data sets. Namely, a named tropical

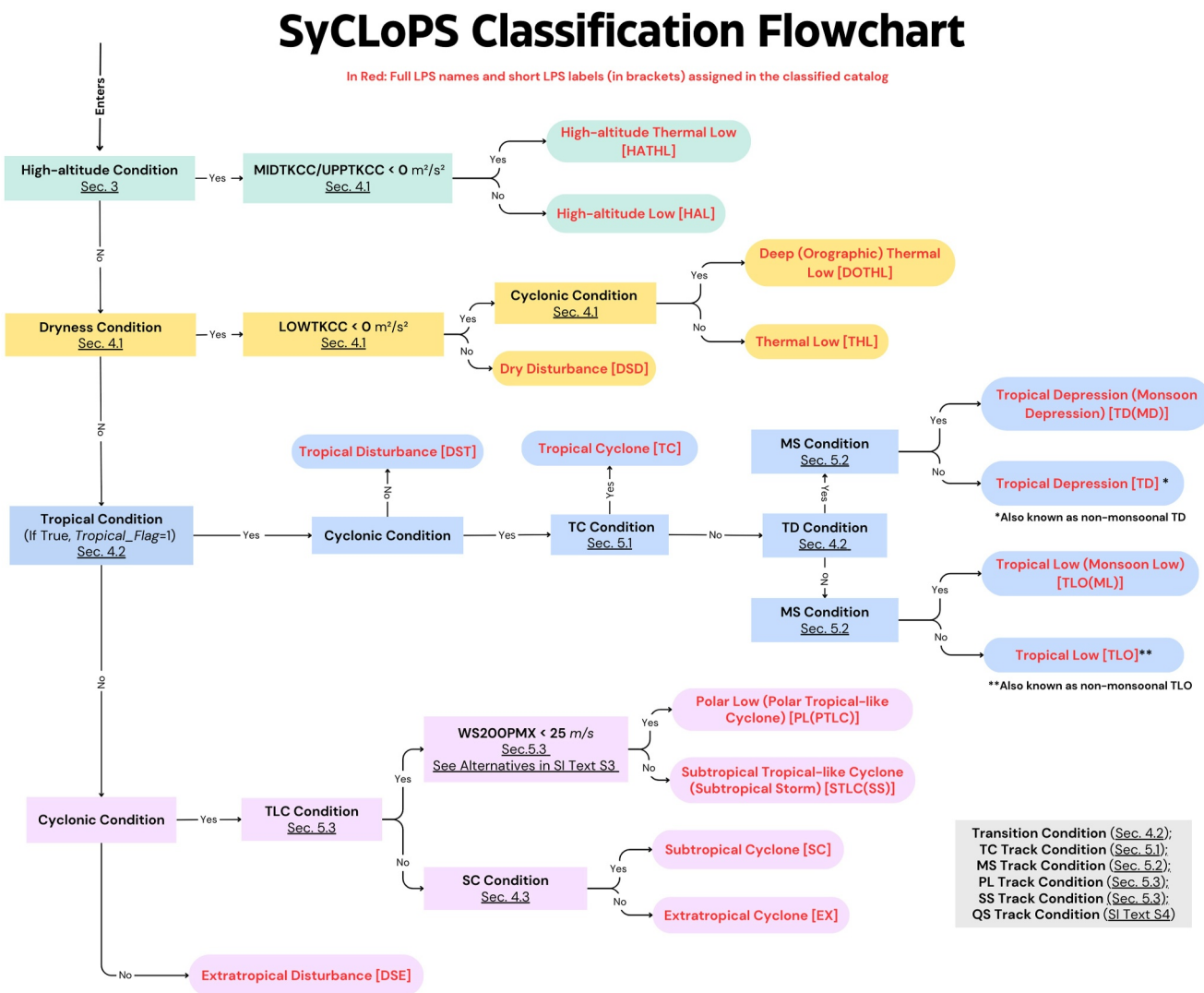

Figure 1. A depiction of the low-pressure system (LPS) classification workflow. The workflow begins in the top-left. A complete list of parameters is given in Appendix C, and a complete list of conditions is provided in Appendix D. Section numbers are noted in the figure below each condition to indicate where details can be found in the text. LPS full names and short labels given by SyCLoPS's output (the classified catalog) are denoted in red.

cyclone will always have a deep warm core, develop in a low-shear environment, and satisfy a certain intensity threshold in all climates. Other important criteria that are potentially more sensitive to global warming are justified in the next section.

Note that we use the LPS catalogs mainly for the purpose of testing our classification conditions for classifying all 16 LPS classes, with an emphasis on TCs (since they are the most influential and well-documented type of LPS). Hence, the provided catalogs may not be the most comprehensive global LPS data set for certain features, as we filter out numerous very weak systems and do not include the smallest and most short-lived systems that are likely to be poorly represented in ERA5 data. Our detection specifications should be enough for general high-impact LPSs; however, some very small and short-lived but detectable high-impact systems, such as certain PLs, can be missed because of the rather large node merging distance (6° GCD), the 18 hr minimum time requirement, or the 3-hourly detection rate. For these cases, users may select their own regions and LPS features of interest and run TE commands with alternative specifications before performing classification. We provide one such example TE command alternation for detecting PLs in the Nordic Seas Text S7 in Supporting Information S1.

Figure 1 shows the LPS classification flowchart. The chart flows from top to bottom through five major branches to disentangle each major class of LPS. Boxes with red texts indicate the final LPS classification full names and

short labels. Details of the conditions applied in the flowchart can be found in Appendix D. The first branch (green) is the high-altitude branch, where we apply the high-altitude condition to extract those LPSs with a surface elevation (ZS) higher than the 850 hPa geopotential height (Z850; typically around 1,500 m) from the input catalog, given that most of the more influential LPSs occur at a lower altitude. Although not as important, some of these high-altitude lows can be major contributors to precipitation over or near plateaus (Li et al., 2019; Tucker, 1999). The second branch (yellow) is the dry branch. In this branch, we segregate those LPSs that hardly produce any precipitation due to their dry low-level circulation. This generally includes thermally-driven shallow thermal/heat low systems, which can affect local cold fronts and heat waves (Reeder et al., 2000; Spengler et al., 2005). Third is the tropical branch (blue), which contains several impactful features such as TCs, MDs and MLs. At this level, the remaining unclassified LPSs will be determined to be tropical or non-tropical based on the tropical condition described in Section 4.2. The fourth branch (purple) is the extratropical branch, where we segregate TLCs (SSs and PLs) and then differentiate SCs from the most typical EXs. Details of the conditions used in the classification process will be discussed further in the next section.

The track conditions found in gray in the bottom-right of Figure 1 are used in the second step of the classification in the Python classifier. They provide additional useful information for reference purposes, but do not affect any LPS node labels assigned in the first step: if a track meets specific track condition(s) using a time step threshold, the track will be labeled as one or more types of the four high-impact LPS tracks in the classified catalog. We also introduce the quasi-stationary (QS) track condition that can identify those LPS tracks that are relatively localized near coastlines or on land so that they can be filtered out or selected when needed. See Text S3 in Supporting Information S1 for information on how we establish the QS thresholds. As there's no hard cut-off between a tropical and non-tropical system, we additionally establish the transition condition along with the tropical condition to define a transition zone to address the ambiguity of the more hybrid and marginal tropical systems potentially under transition. For example, in the "Tropical_Flag" column of the classified catalog, if any LPS node meets the tropical condition (regardless of whether other conditions are met), the value in this column is set to 1.

As shown in Appendix C, extratropical and tropical transition completion (denoted as "EXT" and "TT") nodes are also noted in the classified catalog along with other LPS track information for reference purposes. We define extratropical transition completion nodes as the first LPS nodes along the track with a non-tropical label after the last TC node, and tropical transition completion nodes as the first TC node before the last non-TC node in TC tracks that originate as a non-tropical LPS or within the transition zone defined in Section 4.

4. Justification for Classification Conditions

4.1. High-Altitude and Dry Branch Conditions

In the high-altitude branch, we separate two classes based on the mid-level/upper-level warm core criterion. In this study, we use geopotential thickness to detect the existence of warm cores, similar to the criteria used in Zarzycki and Ullrich (2017) for detecting the upper-level warm core of TCs. Zarzycki and Ullrich (2017) suggested that geopotential thickness is more effective at detecting TCs in climate data than a single-layer temperature criterion because it better captures the full vertical structure of the upper-level warm core. Geopotential thickness is also a smoother meteorological field that is subject to less data noise than single-level temperature. LOWTKCC, MIDTKCC, and UPPTKCC are the negative closed contour criteria of the geopotential thickness between 700 hPa and 925 hPa, 500 hPa and 700 hPa, and 300 and 500 hPa, respectively, over a 6.5° GCD from the maximum thickness within 1.0° GCD of an LPS node. Hence, a threshold of less than 0 $m^2\ s^{-2}$ for these three criteria means that the thickness near the detected location is greater than its surroundings, indicating the presence of a warm core of an LPS. In this case, if MIDTKCC or UPPTKCC is less than 0 $m^2\ s^{-2}$, it indicates that a high-altitude LPS is warm-cored at those levels and may be thermally driven. If this condition is met, the label "High-altitude Thermal Low (HATHL)" is used in the classified catalog; otherwise, the label "High-altitude Low (HAL)" is used.

The dryness condition determines whether an LPS node will enter the dry branch: It requires that average 850 hPa relative humidity over a 2.5° GCD (RH850AVG) is less than 60%. This threshold is determined by the lowest track-maximum RH850AVG (the maximum RH850AVG of all nodes within a track) in the matched PL and SS data set, chosen to prevent misclassification of significant non-tropical systems in the relatively drier subtropical/

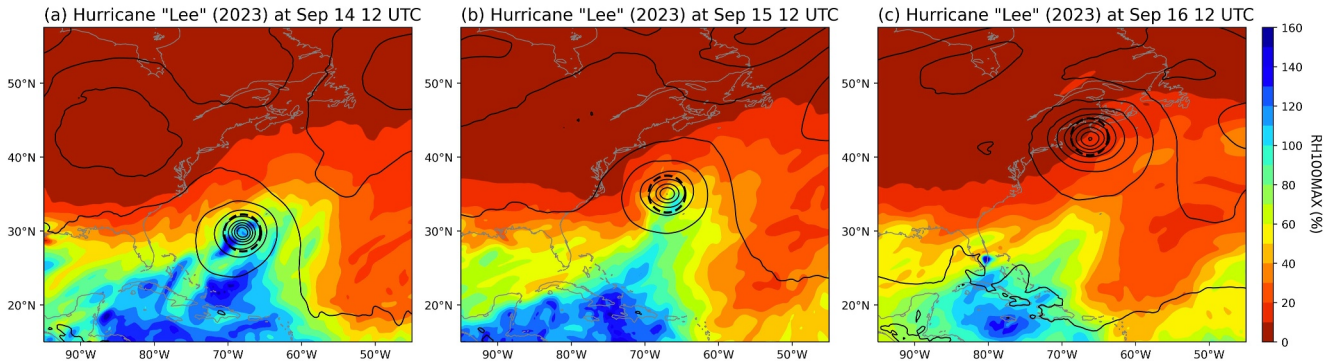

Figure 2. ERA5 Relative Humidity (RH) at 100 hPa during an example of an extratropical transition case (Hurricane "Lee" of 2023) at (a) one day before transition (b) during tranistion, and (c) soon after transition. MSLP is shown using black contours. Note that RH at 100 hPa can exceed 100% in some data sets, reflecting supersaturation.

extratropical regions. Additionally, 850 hPa relative humidity (RH) thresholds are also deemed insensitive to climate change as RH at this level generally responds weakly to surface warming, especially in polar and tropical regions (Lau & Kim, 2015; Merlis et al., 2024; Sherwood et al., 2010). Therefore, we consider RH850AVG at 60% a safe threshold to separate dry convective systems from moist convective systems. Next, the LOWTKCC < 0 m^2 s^{-2} criterion is used to examine LPSs' low-level warm cores. If the condition is not met, the node will be classified as a "Dry Disturbance (DSD)" in the catalog; otherwise, we check the cyclonic condition.

The cyclonic condition uses average 500 hPa relative vorticity over a 2.5° GCD radius (VO500AVG) to determine if an LPS has cyclonic circulation beyond mid-level (i.e., is shallow). A typical heat low is considered to have a dry and warm low-level (between 925 hPa and 700 hPa) core and is shallow (not extending over 500 hPa) in nature (e.g., Hoinka & Castro, 2003; Lavaysse et al., 2009; Smith, 1986). Hence, if an LPS node does not qualify for the cyclonic condition, it will be labeled as a "Thermal Low (THL)" in the catalog. However, some deeper THLs still emerge near elevated topography in the daytime, such as the type II southwest vortex in southwest China (Feng et al., 2016), so the remaining LPSs in the dry branch are labeled "Deep (Orographic) Thermal Lows (DOTHL)."

4.2. Tropical Branch Conditions

The next step in the classification framework focuses on tropical systems. Traditionally, tropical systems such as TCs have been identified using a warm-core criterion (e.g., K. Hodges et al., 2017; Roberts et al., 2020a, 2020b; Zarzycki & Ullrich, 2017). However, in the course of this work we found that this criterion is often satisfied outside of the tropics and leads to many false alarms in the classification. This observation motivated us to examine other fields. We do not consider temperature parameters since they can be thermally-forced by local topography, and various types of LPSs can exist over similar SSTs in the subtropical oceans in different dynamical and thermodynamic environments. Consequently, we found that maximum relative humidity at 100 hPa within 2.5° GCD of LPS node (RH100MAX) is more reliable and flexible for disentangling tropical and extratropical systems as a proxy of "tropicality." There are two reasons that physically ground this choice. First, RH at 100 hPa is distinctly higher in the tropics. This is because only in the tropics is the tropopause often found above 100 hPa, as a result of active moist convection. RH is high there because of the low tropopause temperature and presence of upper-level moisture. RH100MAX also decreases sharply in the subtropics, reflecting the dynamics of the troposphere and the transition between the tropics and subtropics near the edge of the Hadley cells (see Figure S1 in Supporting Information S1 for an illustration of the 1979–2022 global mean RH100MAX). Second, higher RH100MAX values indicate the presence of deep convection associated with a tropical system, and so this parameter is sensitive to extratropical transition scenarios during which it decreases rapidly while TCs gradually lose their deep convective cores and become post-tropical.

To illustrate the behavior of RH100MAX during extratropical transition, we examine a recent extratropical transition case (2023 hurricane "Lee") plotted with RH at 100 hPa in Figure 2. In Figure 2a, the system was embedded in a region of high-level 100 hPa RH two days before transition completion (between 00 and 06 UTC, Sep 15) as defined by the National Hurricane Center. In Figure 2b, less than one day before transition completion,

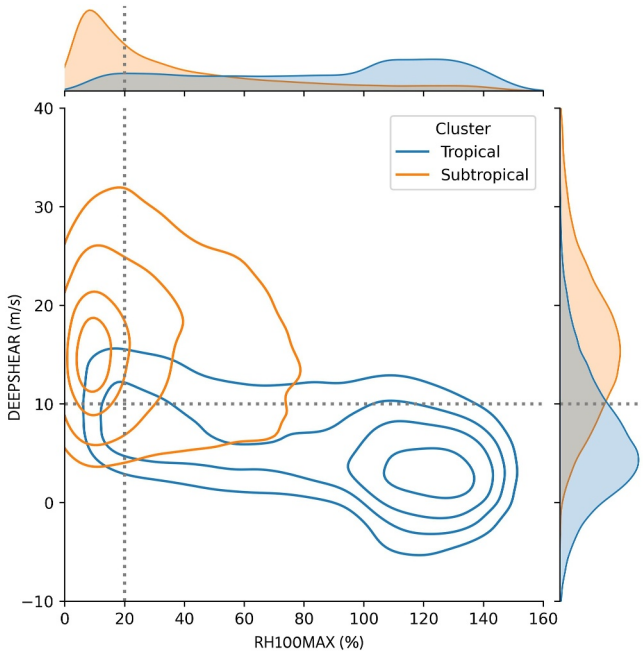

Figure 3. Kernel Density Estimate (KDE) on the RH100MAX-DEEPSHEAR plane for the tropical cluster and the subtropical cluster. The KDE levels are 0.25, 0.5, 0.75, and 0.9. Gray dotted lines indicate the classification thresholds determined by the decision tree classifier.

the surrounding RH had dropped as the hurricane enters the subtropics. However, a belt of higher RH remains stretched out from the deep tropics, indicating the system's remaining "tropicality." RH100MAX is still over 90% at this point, as indicated by the bluish color within the 2.5° GCD circle. In Figure 2c, hours after transition completion, we can see that the 100 hPa environment near the hurricane had become warm and dry, leading to a dramatic decrease in RH100MAX.

In addition to RH100MAX, average environmental deep-layer wind speed shear between 200 hPa and 850 hPa over a 10.0° GCD (DEEPSHEAR) is also used to distinguish tropical systems in the subtropics, especially during extratropical transition. Deep-layer shear is a good physics-related indicator of baroclinicity or an unfavorable environment for tropical deep convection. Post-TCs and general SCs/EXs primarily derive energy from baroclinic sources and are often surrounded by much more intense wind shear compared to tropical systems.

The tropical (and transition) condition with RH100MAX and DEEPSHEAR is constructed as follows. First, we use two LPS node clusters that are hard to distinguish if we were to use a SST-based or warm-core criteria. One node cluster consists of all the matched tropical systems recorded in IBTrACS in the subtropics (the tropical cluster), and the other consists of potential subtropical systems over relatively warm SSTs that are not recorded anywhere in IBTrACS (the subtropical cluster). Note that both clusters (especially the unverified subtropical cluster) will inevitably include some misclassified or transitional LPSs. Details of how we select these two clusters can be found in Text S2 in Supporting Information S1. We then apply the decision tree classifier over RH100MAX and DEEPSHEAR using Gini index splitting criteria to the nodes in the two clusters with a tree depth of 2. Results in Figure 3 show that the tropical and subtropical clusters are best distinguished by a minimum RH100MAX threshold of about 20% (rounded off to the nearest 5%) and a maximum DEEPSHEAR of 10 m s^{-1}, with a best accuracy score of nearly 80%. The accuracy scores mentioned in this article are the best classification accuracy scores a decision tree model can achieve to correctly classify two sets of LPSs given a ground truth. We perform a sensitivity test as demonstrated Text S2 and Figure S2 in Supporting Information S1. The result shows that these two thresholds are relatively stable and insensitive to the SST threshold used for selecting these two clusters. The elongated outer contours of the tropical cluster toward the left in Figure 3 are likely made up of some LPSs near or after extratropical/tropical transition (for reference, about 5% of labels in IBTrACS are "Extratropical"), but also some "drier" tropical systems in drier or less convective basins. For example, while only 6 or 0.6% of Western North Pacific TC tracks have a track-maximum RH100MAX under 50%, 94 or 17% of TC tracks in the North Atlantic fall into this range, with 24 tracks falling under 20%. According to these results, the 20% threshold will serve as the minimum RH100MAX requirement in the tropical condition, and the 10 m s^{-1} threshold will be the minimum DEEPSHEAR requirement in the transition condition, as stronger tropical systems can tolerate a much greater DEEPSHEAR value, such as in many extratropical transition cases. We also notice that DEEPSHEAR of some weak LPSs closer to the equator can slightly exceed the 10 m s^{-1} threshold due to the tropical easterly jet. The cores of tropical easterly jets at 200 hPa are most commonly found near 5° N to 15° N (Lu & Ding, 1989). Hence, we impose that the transition condition will not be triggered when an LPS is within 15° latitudes of the equator.

To find the upper limit of DEEPSHEAR for the tropical condition, we select 883 extratropical transition tracks from the matched TC data sets whose pairs in IBTrACS have a "ET (Extratropical)" or "MX (Mixture, contradicting nature reports from different agencies)" label following the last "TS (Tropical System)" label in the "NATURE" column, and here we define the time of the last "TS" label as the extratropical completion time of each extratropical track. The pre-transition cluster is defined by those nodes that are 3–24 hr before the transition completion, and the post-transition cluster is made up of those that are 3–24 hr after transition completion. We apply the decision tree classifier based on DEEPSHEAR to find the boundary between the two clusters. With an accuracy score of 65%, the results show that the optimal DEEPSHEAR threshold to distinguish the two clusters is

around 18 m s^{-1}. The accuracy score is not high, but it is to be expected—most TCs gradually transform into EXs, suggesting potential subjectivity in their classification. We do not round off the DEEPSHEAR threshold to the nearest 5 m s^{-1} since environmental wind shear typically changes slowly in magnitude along an LPS track. This result is also stable to small changes in the selection of the time range for each cluster.

Finally, we consider 55% as the upper limit of RH100MAX for the transition condition for three reasons: (a) If we apply the decision tree classifier based solely on RH100MAX to separate the tropical and non-tropical cluster, the threshold for RH100MAX will be about 55% with a 74% accuracy score; (b) the median RH100MAX is about 55% at the time of extratropical transition completion as defined above, and (c) the median track-minimum RH100MAX in the matched EW data set (the matched tropical LPS data set with the lowest average RH100MAX) is also about 55%. In summary, the tropical condition refers to RH100MAX > 20% and DEEPSHEAR < 18 m s^{-1}. Upon fulfillment of the tropical condition, the transition condition is satisfied when RH100MAX < 55% or DEEPSHEAR > 10 m s^{-1}, and the latitude is poleward of 15°.

If only the RH100MAX and DEEPSHEAR thresholds are included in the tropical condition, we find that a small number of polar systems could also satisfy the tropical condition. As shown Figure S1 in Supporting Information S1, polar regions can also feature a relatively higher 100 hPa RH that potentially exceeds the RH100MAX threshold in our tropical condition. This is mostly the result of persistent darkness during polar wintertime, which allows the upper air temperature to fall to exceptionally low values despite a lack of moisture. On the other hand, DEEPSHEAR also tends to be quite low in polar regions, as they are not in the main baroclinic zone. It should be fairly easy to further separate these false alarms, since polar regions are not adjacent to the tropics and are therefore distinctly colder. A plot of the air temperature at 850 hPa at the node (T850) distribution for all systems satisfying the RH100MAX and DEEPSHEAR thresholds indicates that tropical systems and polar systems are separate from each other by a ∼15 K (270–285 K) gap (see Figure S3a in Supporting Information S1). Hence, an additional T850 criterion (T850 > 280 K) is included to further distinguish the two systems. Given that the gap that separates the T850 of the vast majority of the polar systems and the T850 threshold is large (∼10 K), and the fact that most of these polar systems reside near the Antarctic continent, where climate cooling has been observed over the past decades (Doran et al., 2002; Oliva et al., 2017), we expect this condition to hold even under worst-case scenarios of global warming, in which the global average temperature is predicted to increase by 4–5 K by the end of the century (Masson-Delmotte et al., 2021).

We also expect the proposed RH100MAX threshold to remain valid under the more extreme global warming scenarios. Merlis et al. (2024) showed that climate model simulations with a uniform +4K SST perturbation results in tropical RH at 100 hPa increasing at a modest rate of 0.5%–1% per 1 K SST warming. This is mainly due to the expansion of the Hadley cells (Sherwood et al., 2010). A fixed RH100MAX threshold will therefore realistically reflect tropical expansion under global warming. RH at 100 hPa in the subtropics and midlatitudes shows even smaller changes (∼0%–0.5% K^{-1}), most likely due to the rising extratropical tropopause (from about 200 to 250 hPa) at a rate of ∼-5 hPa per 1 K surface warming (Lu et al., 2007). In another experiment using 33 climate models, subtropical and midlatitudinal RH at 100 hPa shows an average increase of less than 2% toward the end of the 140-year simulation period during which CO_2 is prescribed to increase by 1% per year (Lau & Kim, 2015). This change is considered minimal given the uncertainties inherent in the chosen threshold.

Further down the tropical branch, the cyclonic condition determines whether an LPS is shallow and so should be tagged as a "Tropical Disturbance (DST)" in the classified catalog. The next step involves the TC condition, which identifies tropical cyclones (TCs) and labels "TC" in the catalog. The conditions for this step are obtained by criterion (parameter threshold) optimization and are discussed in Section 5.1. Tropical depressions (TDs) are sometimes referred to as the weakest TCs before their potential formation. Therefore, the TD condition requires an LPS to at least have weak upper-level warm cores (UPPTKCC < 0 m^2 s^{-2}). We do not require a low-level warm core for TDs as many weaker tropical systems develop a upper-level warm core before a stable low-level warm core is established (Hopsch et al., 2010; Hunt et al., 2016; Reed et al., 1977). We additionally require the greatest positive closed contour delta of MSLP over a 5.5° GCD (MSLPCC55) to exceed 160 Pa, determined by the median LPS node's MSLPCC55 at the IBTrACS track start time of each matched TC track, as agencies tend to start recording LPSs when they are reaching TD wind speed intensities (typically around 20 to 25 knots). Regardless of whether an LPS satisfies the TD condition, the MS condition is also applied to separate monsoonal and non-monsoonal LPSs. The MS condition is obtained by optimization and discussed in Section 5.2. After both the TD and MS conditions have been checked, the classifier assigns one of the four TD and tropical low

(TLO) labels accordingly, as shown in Figure 1. Specifically, monsoonal systems that satisfy both the MS and TD conditions and only the MS condition are considered MDs and MLs and are labeled "TD(MD)" and "TLO(ML)," respectively, in the classification catalog. Similarly, (non-monsoonal) TDs and TLOs that do not satisfy the MS condition are labeled "TD" and "TLO" in the catalog.

4.3. Extratropical Branch Conditions

LPS nodes that do not satisfy the tropical condition are non-tropical (extratropical) systems in the extratropical branch. The cyclonic condition separates "Extratropical Disturbance (DSE)" in the classified catalog before they are examined under the TLC condition obtained by optimization. The criteria for identifying TLC labels in the catalog, which include "SS(STLC)" and "PL(PTLC)," will be discussed in Section 5.3. The remaining LPS nodes will go through the subtropical cyclone (SC) condition which follows the general definition of a typical SC—a non-frontal LPS that features a shallow warm core and an upper-level cold low isolated/detached from the midlatitude westerlies extending its circulation to the surface in the subtropics (U.S. Navy, 1994; Evans & Braun, 2012). Our SC condition states that an LPS must: (a) have a positive closed contour delta of geopotential at 500 hPa over a 3.5° GCD referenced to the minimum value within 1.0° GCD (Z500CC) greater than 0 $m^2\ s^{-2}$ to satisfy the upper-level cold low characteristic; (b) have a LOWTKCC less than 0 $m^2\ s^{-2}$ to guarantee that the low-level is warm-cored; and (c) have the maximum poleward 200 hPa wind speed within 1.0° GCD longitude (WS200PMX) greater than 30 $m\ s^{-1}$ (an effective minimum wind speed for identifying jet streams, see Koch et al. (2006)) to increase the likelihood of the system being equatorward of the polar jet. Since WS200PMX might not be reliable in some regional models, alternatives to WS200PMX criteria used in SyCLoPS are listed and explained Text S4 in Supporting Information S1. We do not require EXs to be cold-cored since many Shapiro-Keyser EXs can be warm-cored due to the warm seclusion in their mature stage (Schultz & Keyser, 2021).

5. Criteria Optimization for High-Impact LPS Detection

As discussed in Section 4, the criteria for TCs, MSs (MDs and MLs), and TLCs all rely on criterion optimization. In this section, we describe the optimization procedure for these four classes of LPS: Specifically, we optimize each type of LPS's detection skill against different skill metrics discussed below to find the best selected parameter threshold combination contingent upon conditions upstream of the workflow. The selection of these parameters is primarily based on physical intuition and previous studies. Since our optimization criteria are based on comparison to subjectively labeled LPS tracks, the optimization procedure also labels LPS tracks by track conditions using the node count parameter (the count of nodes with a specific label within a track) to more stably define an LPS track. Considering that many climate data sets have a 6-hourly temporal resolution (instead of the 3-hourly resolution we are using in this version of the catalog), we start with a minimum node count of 2 during the optimization.

5.1. TC Condition Optimization

The TC condition follows the cyclonic condition in the tropical branch. To identify variables for the optimization procedure, we require the greatest positive closed contour delta of MSLP over a 2.0° GCD (MSLPCC20) to satisfy some minimum value, LOWTKCC to be less than 0 $m^2\ s^{-2}$ (indicating a low-level warm core), and UPPTKCC to satisfy some maximum value in magnitude, since TCs are generally characterized by compact MSLP contours and deep warm cores. We use a MSLPCC20 criterion instead of a maximum wind speed criterion because the latter is much more sensitive to model resolution and can be more easily distorted by complex topography. We also demand the node count of TC-labeled nodes within a track to have some minimum value to define a TC track. Evenly spaced values of these three parameters (over 3,000 combinations) are considered to find the maximum detection skill.

A "test" TC data set is constructed based on each possible 3-parameter combination for the 1979–2021 period, and it is compared to the reference data set IB-TC. A "hit" occurs if the test data set is matched to a track in the reference data set by appearing within 2° GCD from a reference data set data point at the same timestamp. A "miss" occurs if a track in the reference data set does not have a match in the test data set. A "false alarm" is a track found in the test data set but is not matched to any tracks in the reference data set. The TC detection skill metric used here is the hit rate (HR) minus false alarm rate (FAR), expressed as HRMFAR. HR is defined as the ratio of

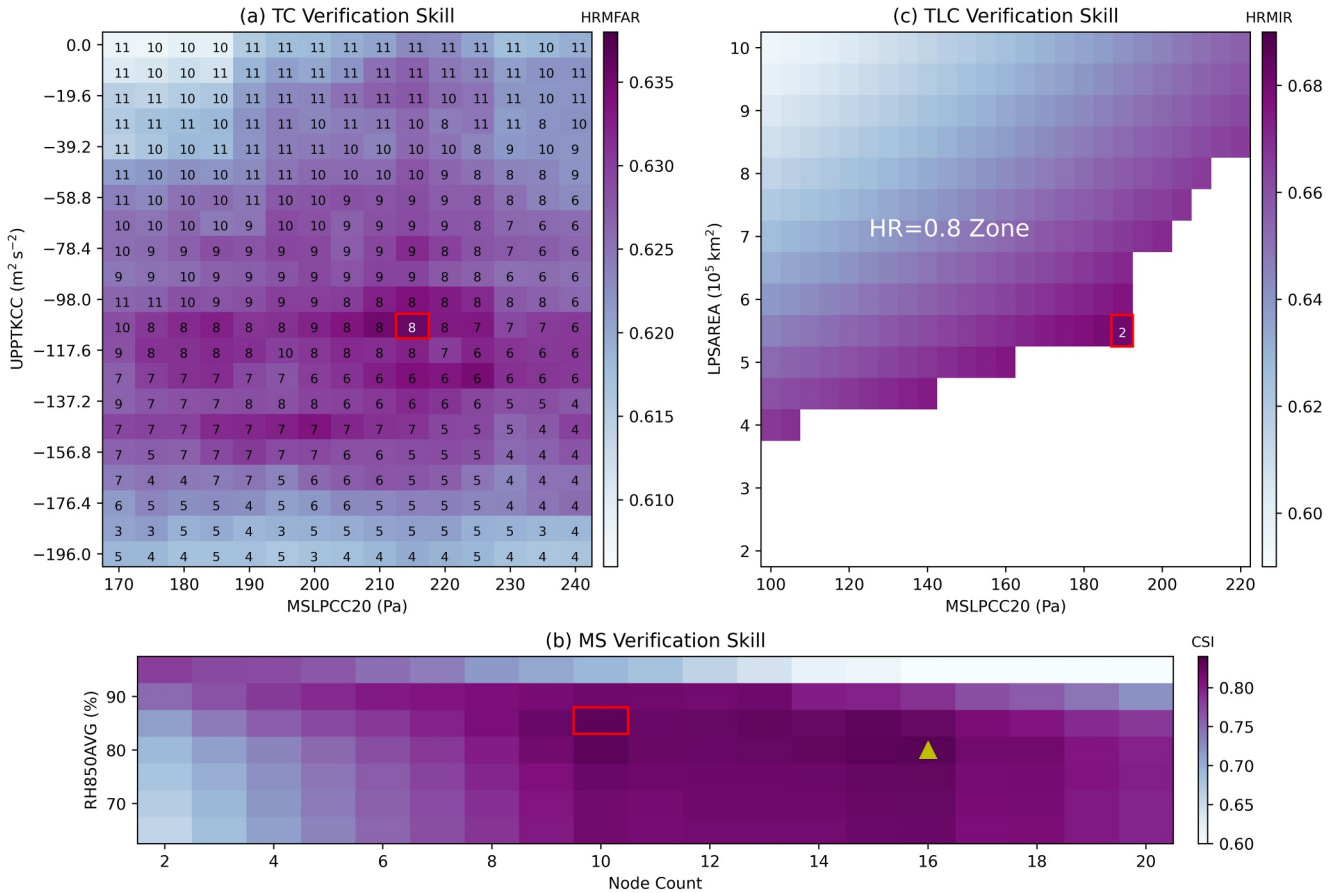

Figure 4. Detection skill optimization for (a) TC, (b) MS, and (c) Tropical-like cyclone using different parameter threshold combinations and detection skills metrics shaded by their metric scores. The numbers in panels (a, c) represent the optimized time step for each combination (the optimal node count in panel (c) is uniformly 2 for every combination). The red rectangle in panels (a, c) indicate where the metric scores are maximized and consequently the final thresholds chosen. In panel (b), the yellow triangle indicates the maximized score, and the red rectangle marks the final thresholds chosen. In panel (c), the metric score shading is only shown for the HR = 0.8 zone.

hits to the total number of hits plus misses, and FAR is defined as the ratio of false alarms to the total number of detected/selected tracks.

Figure 4a shows the detection skill of all chosen combinations of the MSLPCC20 and UPPTKCC thresholds, with the optimal node count shown at the top of each combination. The best detection criteria combination found is UPPTKCC < -107 m^2 s^{-2} (-11 m), MSLPCC20 > 215 Pa (210 Pa is also acceptable since it yields a near-identical score), and TC-labeled node count > 8 with HRMFAR reaching 64%. More Details about the TC detection performance are discussed in Section 6. In summary, UPPTKCC < -107.8m^2 s^{-2} and MSLPCC20 $>$ 215 Pa are used to define the TC condition along with LOWTKCC < 0 m^2 s^{-2}, and the node step threshold specifies that there must be at least 8 3-hourly time steps of TC-labeled nodes within a track for the track to be a TC track (the TC track condition).

5.2. MS Condition Optimization

For MS detection optimization under global detection and without seasonal constraints, we demand criteria that could separate MSs from other weaker tropical LPSs, such as EWs. MSs are considered to be born within monsoon troughs as opposed to the intertropical convergence zone (ITCZ) or upper-level easterly waves. According to National Hurricane Center (n.d.)'s definition, monsoon troughs are characterized by their westerly flow south of the trough, compared to easterly trade winds on both sides of the ITCZ. Furthermore, onsets of regional summer monsoons are often defined as a pattern of a change in wind speed and direction toward stronger westerlies (e.g., Gan et al., 2004; Qian & Lee, 2000). Thus, we develop the U850DIFF parameter, which is the

difference between the weighted area mean of the positive and negative values of 850 hPa U-component wind over a 5.5° GCD. This allows us to determine whether westerly winds (positive U-component wind magnitudes) or easterly winds (negative U-component wind magnitudes) dominate the local 850 hPa environment of a system. The plot of the U850DIFF distribution for the MS and EW matched data sets shows that U850DIFF = 0 m s^{-1} effectively segregates the two clusters (see Figure S3b in Supporting Information S1). Hence, we select U850DIFF > 0 as a minimal requirement for the MS condition.

As implied by the matched MS and EW data sets, MSs in the North Indian Ocean usually have a higher RH850AVG than North Atlantic EWs. This is not surprising, as monsoon regions are generally considered to have more convective activity and larger moisture transport. Given that Vishnu et al. (2020) also used a averaged 850 hPa RH criterion to exclude non-monsoonal systems, we decide to require a minimum RH850AVG threshold in the MS condition.

Critical Sucess Index (CSI) as defined below by Vishnu et al. (2020) is the metric for evaluating MS detection skill.

$$\mathrm{CSI} = \frac{\mathrm{hits}}{\mathrm{hits} + (\mathrm{misses} + \mathrm{false\ alarms})/2} \tag{1}$$

A "hit" here is defined as a track in the test data set having at least one node that is within 3.0° GCD of a track point in the Sikka data set on the same date, and the track must also exist in the matched MS data set. Since TCs are included in the Sikka data set and are considered the most intense monsoon LPSs by the Indian Meteorological Department, tracks that already satisfy the TC track condition and are in the matched MS data set are automatically considered matched (hits). We apply the detection optimization over the same domain and season as Vishnu et al. (2020), except that we incorporate the entire available data period rather than just a portion of it. We compute CSI of all the selected threshold combinations to find where CSI is maximal. The result shown in Figure 4c suggests that the maximum CSI reaches 0.83 for RH850AVG = 80% and MS time step = 16. Our best CSI is thus identical to the value found in Vishnu et al. (2020), in support of the framework's ability to detect weaker tropical systems. We finally choose the second highest CSI (also over 0.83) combination, RH850AVG = 85% and the node count = 10, for the desired thresholds because we would like to include shorter MS tracks. Following these results, the MS condition is set as RH850AVG > 85% and U850DIFF > 0 m s^{-1}, and a track is considered to be a MS track only if 10 or more of its 3-hourly nodes satisfy the MS condition and are labeled as "TD(MD)" or "TLO(ML)" in the classified catalog. The MS track label highlights those weaker tropical LPS tracks that are more stably labeled as monsoonal systems, although they can also coincide with TC-labeled tracks (i.e., TC tracks detected by SyCLoPS) per our standards. EWs and other tropical waves are likely to be included in the non-monsoonal TDs/TLOs that fall short of the MS condition, as well as other weak LPS classes (i.e., tropical/dry disturbances). One may assume that westward-propagating disturbances and non-monsoonal TDs/TLOs that meet the tropical condition (indicated by "Tropical_Flag = 1" in the classified catalog) and are not in MS-labeled tracks are mainly easterly waves.

5.3. TLC Condition Optimization

"Tropical-like cyclones" refers to non-tropical LPSs that resemble "real" TCs in certain ways. For instance, a mature Mediterranean hurricane may have a distinct eyewall and a deep warm-core structure despite lower SSTs and greater baroclinity in a non-tropical environment (Pytharoulis et al., 2000). PLs (sometimes referred to as intense polar mesoscale cyclone or Arctic hurricanes) and Mediterranean hurricanes (a branch of SSs), although still vaguely defined, may all be described as a group of mesoscale (small), intense, and short-lived (in terms of their TLC-stage lifespan) LPSs that can be classified as "tropical-like." Based on the definitions mentioned in Section 2, the most noticeable difference between PLs (PTLCs) and SSs (STLCs) might be that PLs develop north of the polar front or the main baroclinic zone in cold air masses, compared to SSs emerging from the subtropics. The term "hurricane-like extratropical cyclone" is also used in Romero and Emanuel (2017) to group Mediterranean hurricanes and North Atlantic PLs together. Here, we adopt a similar view that SSs and PLs are comparable to one another but different from typical extratropical/subtropical cyclones and could be flagged under the same TLC condition. The conventional definition of PLs as being north of the polar front can then be used to distinguish between them. Under this framing, SyCLoPS offers a means for the first objective global identification of all TLC systems in climate data.

Since a minimum requirement of near gale-force wind intensity similar to TCs is required to define SSs and PLs, similar parameters such as MSLPCC20 and LOWTKCC are used to detect TLCs as we did to detect TCs. We expect TLCs to have, on average, a shallower/weaker warm-core structure compared to TCs. Hence, we first impose a minimum requirement for the two warm core criteria (LOWTKCC < 0 m^2 s^{-2} and MIDTKCC < 0 m^2 s^{-2}). Static-stability or open-water criteria used in previous PL detection studies (Stoll, 2022; Stoll et al., 2018; Zappa et al., 2014) are not considered here as they appear too restrictive to global TLC detection. For example, PLs may also appear closer to the baroclinic zone in a more sheared environment (Montgomery & Farrell, 1992; Terpstra et al., 2016), and intense storm activity can often occur over Antarctic sea ice (Hepworth et al., 2022). The other significant distinction of TLCs is their small or mesoscale sizes. Thus, we generate LPS size blobs and compute the LPS size (extent) measured by the LPSAREA parameter as described in Appendix E, in addition to the parameters directly computed by TE to evaluate the defined two-dimensional size (area) of LPSs.

We use the combined matched SS and PL data set, which consist of 174 tracks, as our reference data set for optimization. We concede that it's difficult to evaluate or compare global TLC detection skills because credible TLCs' records are limited and regional in scope, and their definition inexact. To overcome this, we first remove 12 tracks in the reference data set that have a track-maximum MSLPCC20 lower than 215 Pa (the MSLPCC20 standard for TCs) to further avoid including tracks that are too weak to be considered TLCs. Second, we acknowledge that some TLCs could be embedded within a synoptic-scale circulation or trough in the background, sometimes with a twin low nearby (see Figure S4 in Supporting Information S1 for an example), and thus will appear large (or be zero if embedded in a system with lower MSLP) using our size computation method. To work around this observation, we determine that LPSs with MSLPCC20 $>$ 420 Pa (90% percentile of detected non-tropical, non-shallow LPSs' MSLPCC20) and a ratio of MSLPCC20 to MSLPCC55 greater than 0.5 (reflecting the presence of a dominant and more compact LPS core within the larger system) satisfy the embedded TLC alternate criterion and are exempt from the LPSAREA requirements. Third, since the scope and quality of the reference data set is constrained, FAR becomes rather meaningless and is replaced by the infrequency rate (given that TLCs are infrequent), defined as the fraction of selected TLC tracks among all detected tracks that have at least one node that passes the cyclonic condition in the extratropical branch (a 0.1 infrequency rate as defined would correspond to a 45 occurrence per month in this SyCLoPS LPS data set). Hence, the detection skills metric we use for the TLC condition is the HR minus infrequency rate, or HRMIR. Here, HR is simply defined as the fraction of tracks that are detected (hits) in the reference data set. Given the limited sample size, HR is rounded to the nearest tenth (i.e., 0.750 and 0.849 will be rounded to 0.8) to roughly reflect its 90% confidence interval (CI) and potential sampling errors.

We iterate the selected range of MSLPCC20 and LPSAREA threshold combinations for TLC condition optimization. The best HR attained is at the 0.8 level as shown by the shading in the upper left zone of Figure 4b. Within this zone, the TLC condition is optimal when IR is the smallest (11.9%) at MSLPCC20 $>$ 190 Pa and LPSAREA $< 5.5 \times 10^5$ km^2 (given that LPSAREA is nonzero) on top of the other thresholds we mentioned above. The LPSAREA threshold chosen here agrees with the meso-α scale range (i.e., roughly a 400–500 km LPS radius), which aligns with the upper size range of many studied TLCs (e.g., Fita et al., 2007; Holland et al., 1987; Noer et al., 2011; Rasmussen & Turner, 2003). Due to the short-lived nature of TLCs, HRMIR in all combinations maximizes when the node count equals 2. LPS nodes that have been tagged as TLC will then be further classified as PLs or SSs depending on whether they are located further north to the polar jet (WS200PMX < 25 m s^{-1}). Tracks with 2 3-hourly TLC-labeled nodes (PL or SS) and at least one PL or SS-labeled node are then assigned "PL(PTLC)" or "SS(STLC)" track labels. For an alternative test, we remove the embedded TLC criterion and perform the optimization. The results show an identical HR, a slightly lower IR, and 72% overlapped detected TLC tracks (i.e., LPS tracks picked up by both TLC detection algorithms) when MSLPCC20 $>$ 145 Pa and LPSAREA $< 7.0 \times 10^5$ km^2. Thus, it may be treated as an alternative TLC condition, although it risks excluding many embedded TLC nodes.

6. Results and Applications

6.1. Main Results

In Figure 5a, we plot the kernel density estimate (KDE) on the RH100MAX-DEEPSHEAR coordinate of all 6-hourly sampled LPS nodes that have passed the second (dry) branch and meet the cyclonic condition to verify the

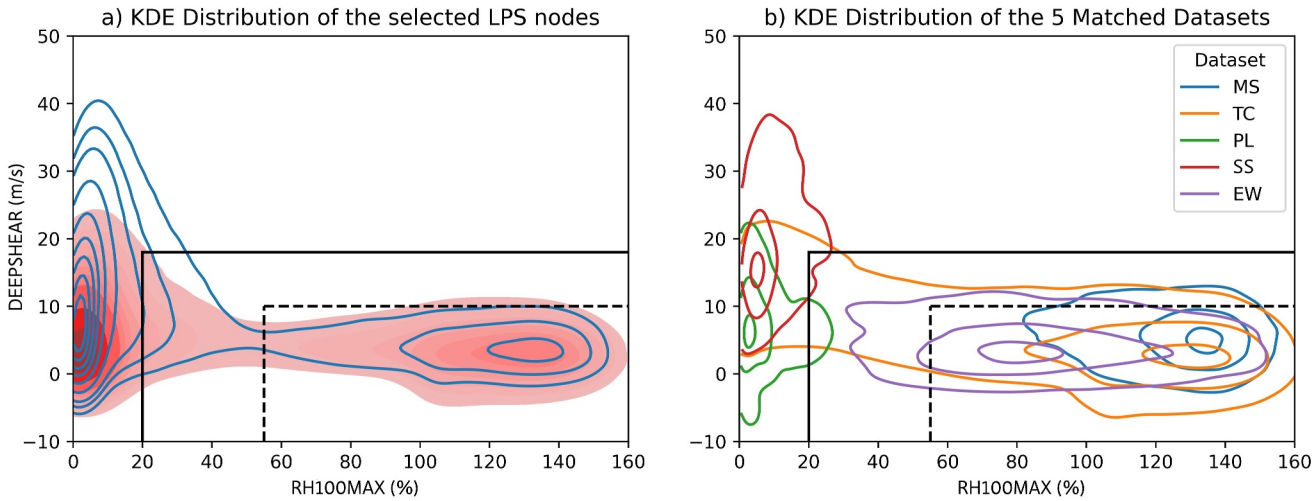

Figure 5. (a) The 10 KDE levels evenly distributed between 0 and 1 of all the selected detected low-pressure system (LPS) nodes (blue contours) and the warm-core LPS nodes (red filled contours); and (b) the 3 KDE levels set at 0.1, 0.5, and 0.9 of the five matched data sets on the RH100MAX-DEEPSHEAR coordinate.

efficacy of our tropical and transition conditions. Our results demonstrate the validity of using RH100MAX and DEEPSHEAR thresholds as the foundation for these conditions. The KDE clearly depicts two main clusters, separated by RH100MAX and DEEPSHEAR. The solid-line and dash-line boundaries delineate the tropical and transition conditions. The RH100MAX transition threshold cuts through the narrowest part of the KDE. The cluster centered inside the tropical condition bounds is the tropical system cluster, while the cluster centered outside the box is the non-tropical system cluster, which is apparent from Figure 5b, where the KDEs of the five matched data sets are placed on the RH100MAX-DEEPSHEAR coordinate. Within the tropical system cluster, the TC cluster spans the widest range as it includes LPSs undergoing extratropical transition and at post-TC stage, whereas the MS and EW clusters have the highest and lowest mean RH100MAX values respectively. Most of the matched tropical LPSs are within the transition boundaries (which may be deemed as the deep tropics). Inside the non-tropical system cluster, the SS cluster has a higher mean DEEPSHEAR value than the PL cluster. The red filled contours in Figure 5a depict the KDE of warm-core systems, defined as the previously selected LPS nodes that meet the criterion of UPPTKCC < -58.8 m^2 s^{-2} (-6 m). The KDE shows that systems with a upper-level warm core can exist in both tropical and non-tropical clusters, and thus, the warm-core criteria may not be ideal for classifying LPSs across the spectrum. According to the classified catalog, the vast majority of the labeled tropical systems are confined within 40 degrees of the equator.

SyCLoPS LPS labels are generally in good agreement with the labels in IBTrACS. Two types of labels are provided in IBTrACS: first, the labels in the "NATURE" column assigned by global WMO agencies, and second, the labels assigned by US meteorological agencies in the "USA_STATUS" column. The WMO labels are more general than the USA labels, as the USA labels include more classes based on LPS intensity. Miscellaneous labels that are vaguely defined and have a small sample size are not included in the comparison. Information about the two agencies' labels can be found on the IBTrACS website and in Landsea and Franklin (2013). Labels are compared when LPS nodes in our data set and IBTrACS track points lie within 2.0° GCD of each other at the same timestamp. Figure 6 shows the probability of success (POS) for correctly labeling an LPS node of a particular class (setting IBTrACS labels as ground truth). Overall, 95% of the matched nodes are in agreement with the WMO labels, mainly contributed by the high "TS" POS of 97% (WMO's "TS" label refers to "tropical system"). Since WMO's "DS (disturbance)" label also exists, we regard "TS" as all non-shallow tropical systems, which is equivalent to all tropical system labels but "DST" in our labeling system. This result suggests that very few tropical systems are mistakenly labeled as non-tropical systems by our classification. The extratropical system POS is at 78% when we compare labels in the extratropical branch to the "ET (extratropical)" label of WMO. The majority of the extratropical records in IBTrACS are post-TCs immediately after extratropical transition. Therefore, it suggests a rather small error in the extratropical transition completion time justified by our classification when compared to IBTrACS. Breaking down the tropical systems, our TC POS remains at a relatively high level of 74% against TC labels given by USA agencies, while TD (which includes TD and MD) has a much

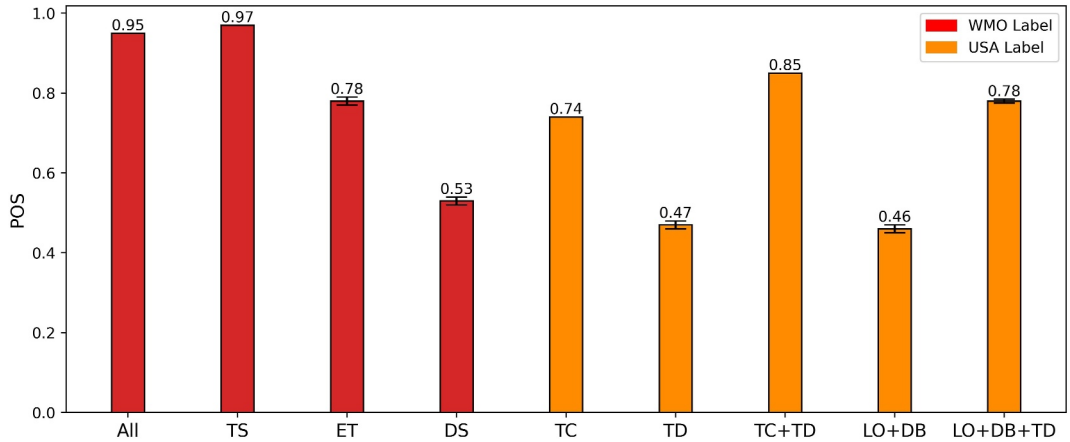

Figure 6. Probability of success (POS) of our labels when compared to labels given by WMO (red bars) and USA agencies (orange bars). See text for details. POS values are shown on the top of bars with 95% confidence level error bars denoted.

lower POS of 47%. We find that TDs are almost equally likely to be misclassified as TCs and tropical lows (TLOs and MLs), which reflects ambiguity in their definitions and inevitable biases in LPS intensity evaluations by agencies, reanalysis, and our classification. If TD is considered a category of TC for both our and IBTrACS labels, the POS of "TC + TD" rises to 85%. The weakest system labels in IBTrACS, including "LO (low)" and "DS/DB (disturbance)," are more vaguely defined. They are often used at the start of TC tracks, and the labeled LPSs may not have a discernible surface center (Landsea & Franklin, 2013; National Hurricane Center, n.d.). Hence, we treat them as the same label, which is equivalent to TLO systems (TLO and ML), disturbances (DST, DSD and DSE), and thermal low systems (THL, DOTHL, and HATHL) in our labeling system. Probability of success of about 50% is realized for this category compared to labels of WMO and USA agencies. Similarly, they are subject to biases in intensity evaluations and their exact definitions. When TDs are included in this class for both our and IBTrACS labels, the POS increases to 78%.

TC detection skill is improved using SyCLoPS's TC track labels when compared to the previous TE algorithm (the Zarzycki & Ullrich method; Zarzycki & Ullrich, 2017). For the Zarzycki & Ullrich method, TC tracks are identified when nodes in a track that satisfy UPPTKCC < -58.8 m^2 s^{-2} (-6 m), MSLPCC55 > 200 Pa, WS (maximum wind speed at 10 m within 2.0° GCD) > 10 m s^{-1}, and ZS < 150 m^2 s^{-2} are detected for at least 54 hr equatorward of 50° latitude. We resample the detected TC data set to match the 6-hourly data frequency of IBTrACS. The HRMFAR of Zarzycki & Ullrich is computed against the same IB-TC data set for the period of 1979–2021 using the same definition of hits and false alarms mentioned in 5.1. Table 2 summarizes the TC detection skill metrics of both methods. The mean start (end) time differences in the table refer to the time differences between the start (end) time of the detected TC track and the corresponding IB-TC track's start (end) time. To summarize, the detection skill improvements are: (a) HRMFAR is increased by 7.5% due to a 5.5% decrease in FAR and a 2% increase in HR; and (b) the early detection of the pre-TC stage and late detection of the post-TC stage are significantly improved, extending TC track length by an average of 136 hr. The effects of these improvements are revealed in Figure 7. Tracks detected using SyCLoPS are visibly longer at both ends (the pre-TC stage and the post-TC stage) compared to those tracked by the Zarzycki & Ullrich method. Notably, the new approach more closely matches IBTrACS observations in the South Atlantic and the Southeast Pacific, among other subtropical oceans, by largely reducing false alarms in those regions. We also notice that many official wind data in IBTrACS's tracks are missing in earlier years in basins of the Indian Ocean (so they are not included in IB-TC) due to the fact that some agencies did not accept their regional responsibility until the early 1990s. Hence,

Table 2
Detection Skill Comparison Between SyCLoPS and the Zarzycki & Ullrich Method

Method	HR	FAR	HRMFAR	Mean start time difference (hr)	Mean end time difference (hr)
Zarzycki & Ullrich	76.2%	20.1%	56.1%	28	−30
SyCLoPS	78.2%	14.6%	63.6%	−49	28

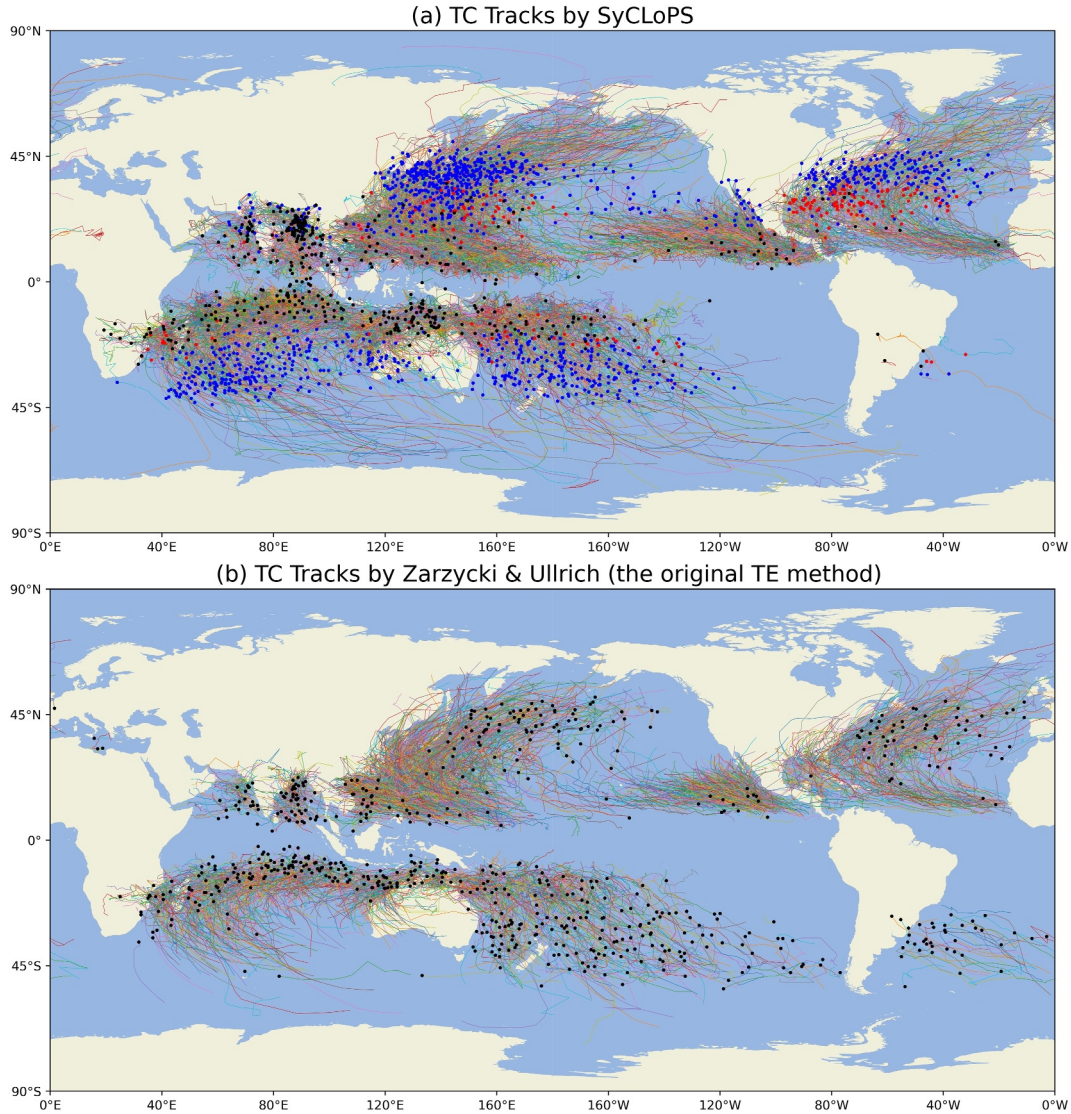

Figure 7. 1979–2021 TC tracks as tracked by (a) SyCLoPS, and (b) the Zarzycki & Ullrich method. Black dots are the first locations of false alarm tracks. Blue and red dots are extratropical and tropical transition completion locations indicated by SyCLoPS. 1337 extratropical transition cases and 195 tropical transition cases are detected.

many false alarms in the tropical Indian Ocean for both methods could actually be real TCs (hits). Discrepancies in wind measurement standards, observations, and operational procedures among agencies for different basins are also noted in Schreck et al. (2014), suggesting the presence of a "TC gray zone" due to these biases—that is, a range of parameter values where different experts would draw different conclusions on the classification of a feature. Therefore, perfectly matching a subjective TC data set is likely impossible. The blue and red dots show the extratropical and tropical transition completion positions of applicable TC tracks indicated by the classified catalog. About 40% of the identified TC tracks undergo extratropical transition, which is comparable to the global extratropical transition fractions using a CPS method reported in Datt et al. (2022). We compare the detected TC tracks of SyCLoPS that have a match to an extratropical transition case recorded in IBTrACS and find that SyCLoPS detects 87% of all such extratropical transitions with an average (median) error of +10 (+6) hours in the transition completion time (i.e., the timestamp of the first labeled extratropical node after the TC stage). The HRMFAR of this new algorithm may be further elevated through post-processing operations such as eliminating QS tracks or marginal TC tracks that primarily reside in the transition zone. We advise being cautious when eliminating any marginal TCs since they can reside in the "TC gray zone." As an example, the 2001 Australia "Duck" is a classic marginal TC (see Garde et al., 2010). Although this storm was not recorded by the agency and

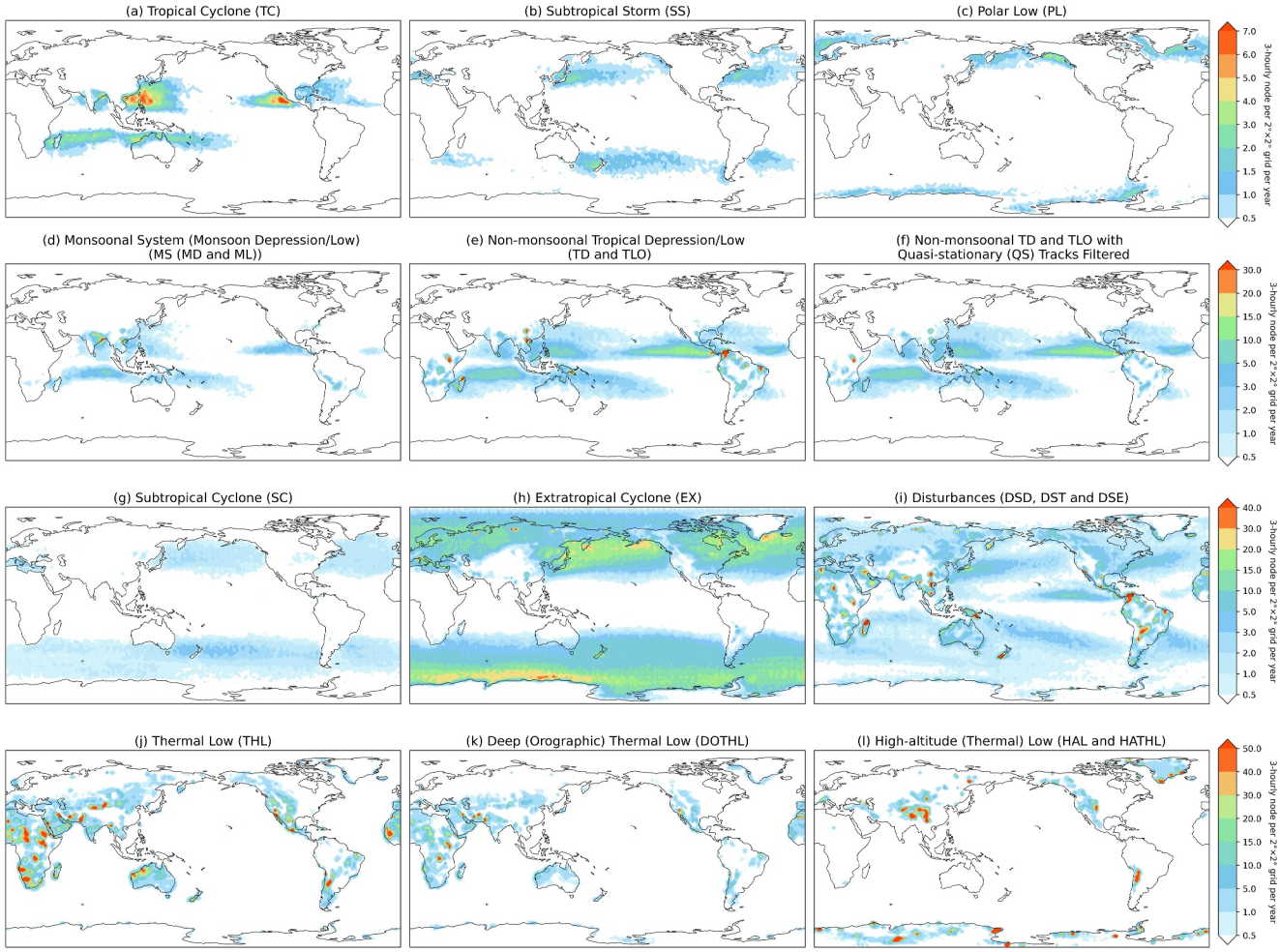

Figure 8. 1979–2022 annual frequency of (a) tropical cyclone (TC), (b) subtropical storm (SS), (c) polar low (PL), (d) monsoonal system (MS (MD and ML)), (e) non-monsoonal tropical depression (TD) and tropical low (TLO), (f) same as (e), but with quasi-stationary (QS) tracks filtered, (g) subtropical cyclone (SC), (h) extratropical cyclone (EX), (i) disturbances (DSD, DST and DSE), (j) thermal low (THL), (k) deep (orographic) thermal low (DOTHL), and (l) high-altitude LPSs (HAL and HATHL) as measured by 3-hourly nodes per 2° × 2°grid.

it does not satisfy our TC track condition, it is labeled as "TC" at four time steps under our classification. See Figure S8 in Supporting Information S1 for a labeled track map of this special case.

Major globally detected LPS annual frequencies for the different classes of LPSs are shown in Figure 8. In general, the frequencies of these systems are in accordance with observations. Please refer to Figure S5 in Supporting Information S1 for a frequency bar plot of all LPS classes. The first row of Figure 8 contains the least frequent LPS classes, followed by MS in the second row, which are all high-impact LPSs that can be considered extremes. TC frequencies are consistent with their track activity in the tropics and during extratropical transition (Figure 8a). In Figure 8b, SSs are more frequent in the Mediterranean Sea, the most studied hotspot for these features. They are also commonly found in the storm-track regions (Western North Pacific and the northwestern Atlantic, as defined in Blackmon et al. (1977)), the southwest Atlantic, the southeast Pacific, the Japan Sea, and the Tasman Sea close to Southeast Australia. Those regions are all well known for their intense or tropical-like LPS activities, which include Australian east-coast cyclones, Chilean storms, Japanese south-coast explosive cyclones, TLCs/mesocyclones in the Sea of Japan and the Yellow Sea, and subtropical storms across the Atlantic (see e.g., Cavicchia et al., 2018; Gozzo et al., 2014; Guishard et al., 2009; Heo & Ha, 2008; Iwao et al., 2012; Shimada et al., 2014; Winckler et al., 2017). We expect that the successful classification of subtropical storms is effective for reducing TC false alarms in the SyCLoPS framework. PL activity reaches as far south as the Sea of Japan, and they are most prevalent in the Nordic Seas, the Gulf of Alaska, and over or near the sea ice of the

Southern Ocean (Figure 8c). Intense post-TCs are sometimes classified as TLCs in our framework, and removing them has only a minor impact on the frequencies of SSs and PLs. MSs are mainly constrained in the tropical monsoon region defined in Li and Zeng (2003) and have two evident hotspots in the North Indian Ocean and near the Gulf of Tonkin in the South China Sea (Figure 8d). Non-monsoonal TLOs and TDs are found throughout the tropics, with some overlap with MS activity and evidence of QS tracks shown by localized high frequencies mainly near rainforest regions (Figure 8e). After filtering those QS tracks labeled by the QS track condition, strong LPS occurrences largely disappear, leaving other features mostly untouched. SCs are more widespread but less concentrated compared to SSs (Figure 8g). EX is the most common type of LPS labeled, and it is omnipresent outside of the tropics (Figure 8h). Disturbances are found globally across latitudes, and THLs and DOTHLs are located primarily on arid lands (Figures 8i–8k). Finally, high-altitude LPSs occupy mountainous areas, including parts of the Antarctic continent (Figure 8l).

We show the vertical cross section composites at the latitude of LPS's center for the six selected LPS classes labeled by SyCLoPS in Figure 9. TCs feature a classic dumbbell-like structure resembling the shape of a cumulonimbus, as indicated by the two RH maxima at the lower- and the upper-level (Figure 9a). Diabatic heating or latent heat release in TCs, as suggested by the cyclonic potential vorticity (PV) contours, is evident throughout the lower-level and upper-level. The deep warm-core structure suggested by the potential temperature contours is most evident in the TC composite. Figure 9b shows that a typical THL features a classic warm and dry low-level core, which is largely constrained to the boundary layer. As shown in Figures 9c and 9d, weaker tropical systems have far less developed convection and warm cores compared to TCs. MSs have comparatively higher RH at each level and a slightly more developed lower-level circulation than other typical TDs/TLOs. An eastward tilt of the RH field below 300 hPa is also noticeable in the non-monsoonal TD and TLO composite in Figure 9d. Cyclonic PV contours stretching down from the subtropical tropopause in the SS composite (Figure 9e) imply that some SSs undergo a downward development pathway, extracting cyclonic PV from upper-level PV anomalies or PV streamers, which agrees with the Mediterranean hurricane development mechanisms described in Flaounas et al. (2022). The warm core and the diabatic heating are more constrained to the lower level for PLs, as depicted in Figure 9g. The global patterns (Figures 9e and 9g) of SS and PL also appear to have less noise (induced by local topography) and an enhanced PV signal in the vertical structure of SS and PL compared to the patterns (Figures 9f and 9h) represented by regional SSs and PLs associated with the records in the subjective SS and PL data sets. Despite the fact that both TCs and TLCs (SSs and PLs) have relatively deep warm cores, the upper-level RH of SSs and PLs (as shown in Figures 9e and 9f) is significantly lower than that of TCs and other tropical systems. This distinction supports our choice of the RH100MAX criterion in the tropical condition.

6.2. Other Applications

We now show some simple applications based on the classified catalog produced by SyCLoPS. One major benefit of SyCLoPS is that it can reveal a fairly complete history of each LPS track, so that the evolution of an LPS can be effectively traced. Thus, a useful application is showing a track along with its labeled nodes, such as the example in Figure 10. The example depicts the track history of the Western North Pacific typhoon Mindulle in 2021. Mindulle is first detected as a disturbance near the equator, then gradually intensifies as a non-monsoonal TLO/TD before it becomes stably labeled as TCs. It completes its extratropical transition around 40° N and later develops into a SS and PL before dissipating as a EX in Alaska. The genesis time (the first TD label time), the first TC record time, and the transition completion time are all within 12 hr of the corresponding IBTrACS records, while the record given by SyCLoPS further extends the IBTrACS track length. A phase diagram displayed by the DEEPSHEAR-RH100MAX coordinate is attached to the figure. The phase evolution shows that the RH100MAX of the TC stays at a high level while the environmental wind shear gradually increases. The system's RH100MAX decreases sharply during extratropical transition, which is completed when the TC no longer satisfies the DEEPSHEAR criteria from the tropical condition. In its final stage, the system enters a lower-sheared environment with very low RH100MAX. More examples like this of different LPS classes (including North Atlantic hurricanes, the "Duck," an MS, and TLCs) can be found in Figures S7–S9 in Supporting Information S1.

The labeled nodes can also be combined with the LPS size blobs we generated when computing LPSAREA to derive the accumulated integrated kinetic energy (IKE; Powell & Reinhold, 2007) of targeted LPSs. Figure S6 in Supporting Information S1 shows an illustration of the labeled LPS size blobs. IKE is directly correlated with the potential destructiveness of LPSs, as it takes the size parameter into account. The IKE of an LPS is defined as the 1 m-deep mean kinetic energy at the surface level (here approximated by the 925 hPa level) within the LPS extent

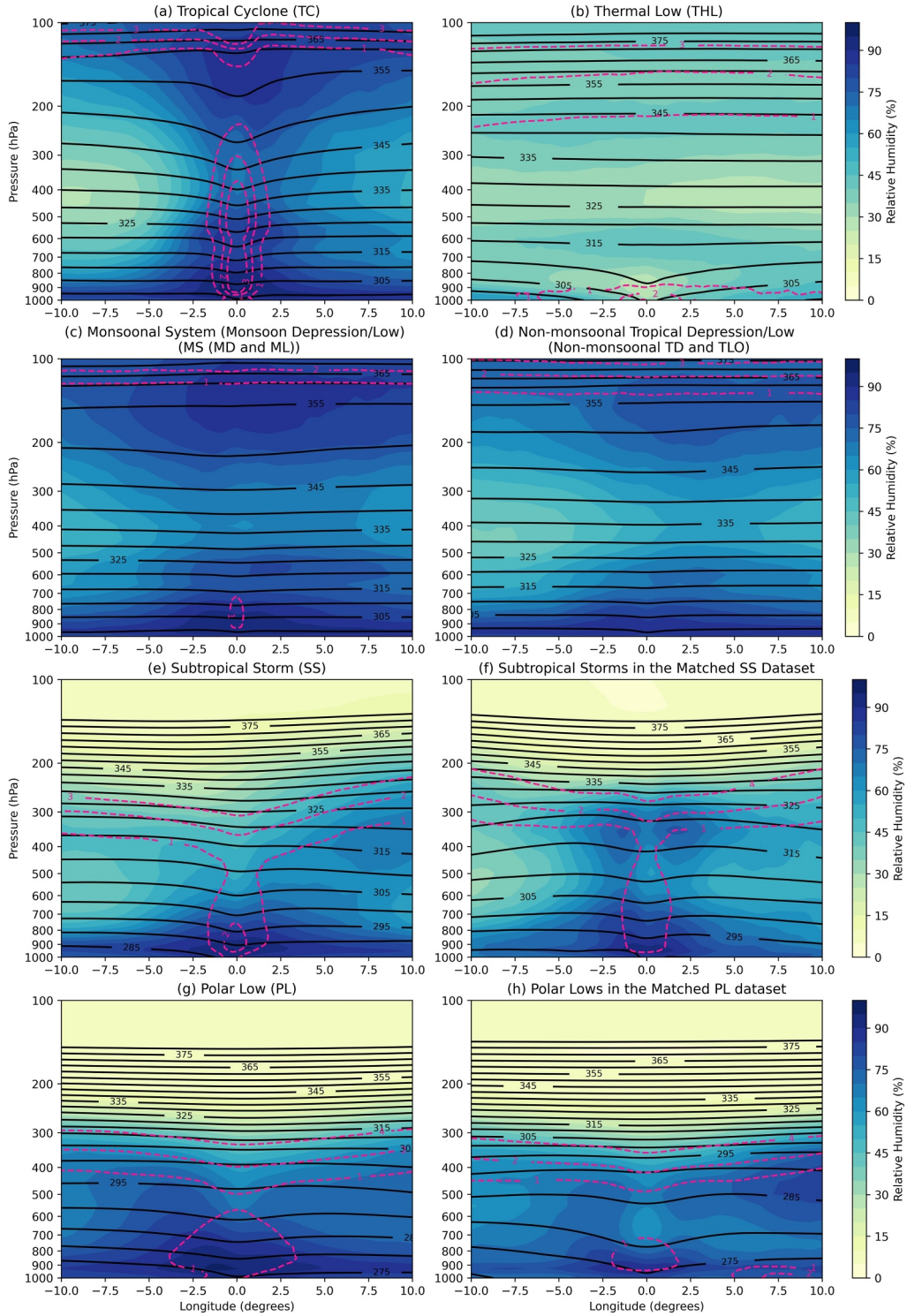

Figure 9. Vertical cross section composites of low-pressure system (LPS) node classified as (a) tropical cyclone (TC), (b) thermal low (THL), (c) monsoonal system (MS (MD and ML)), (d) non-monsoonal tropical depression (TD) and tropical low (TLO), (e–f) SS and SSs in the matched-SS data set, and (g–h) PL and PLs in the matched-PL data set. Dark pink dashed lines are contours of cyclonic potential vorticity (unit: PVU $\left(1.0 \times 10^{-6}\ \mathrm{m^2\ s^{-1}\ K\ kg^{-1}}\right)$), and black contours are potential temperature (K). The TC, MS, SS and PL composites are each based on 1,000 randomly chosen nodes tagged with the specific type of label in the specific type of LPS track (i.e., 1000 TC-labeled nodes in TC-labeled tracks). The non-monsoonal TLO/TD composite is based on 1,000 randomly chosen nodes labeled "TLO" or "TD," except those in MS or QS tracks. The THL composite is based on 1,000 randomly chosen THL-labled nodes.

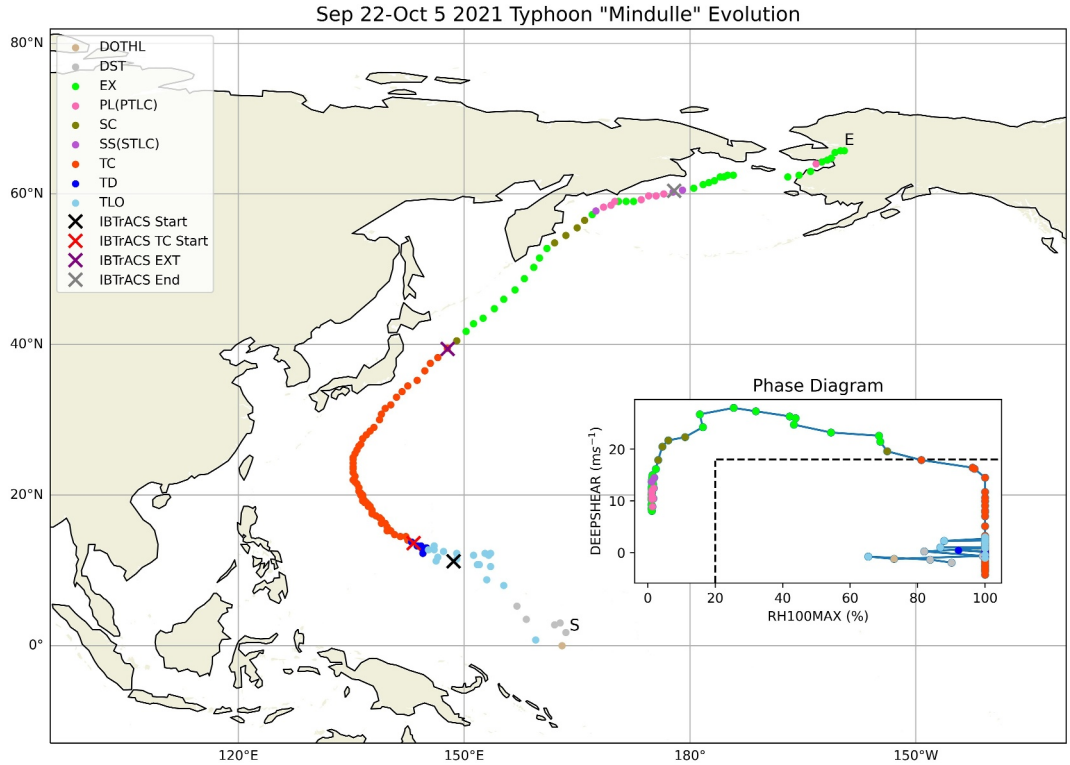

Figure 10. An example of different low-pressure system labels in a TC (2021 Typhoon "Mindulle") lifetime. The phase diagram shows its evolution on the RH100MAX-DEEPSHEAR coordinate with the tropical condition threshold outlined in dashed lines. We convert all instances of supersaturation of RH100MAX to 100% in the phase diagram. S and E indicates the start and the end of the track. The cross marks indicate the position of the start of IBTrACS record (black), the first IBTrACS TC record (red), IBTrACS extratropical transition completion (purple), and the end of IBTrACS record (gray).

we define for LPSAREA. Accumulated IKE of an LPS can be useful to study trends in LPS activity (Kreussler et al., 2021). In Figure 11, we show the accumulated IKE (in trillion joules, TJ) of the four types of high-impact LPS nodes from 1979 to 2022. Specifically, blobs associated with TCs (TC nodes) in TC-labeled tracks, TDs and TLOs (MD, ML, TD and TLO nodes) in MS-labeled tracks, SSs in SS-labeled tracks, and PLs in PL-labeled tracks are selected, respectively, for their IKE accumulations. The results indicate that TCs have the most widespread and severe wind impact over land, while the kinetic energy of MSs accumulates the most along the coast of the Bay of Bengal. SSs are kinetically active in several hotspots globally. The influence from their winds extends to places including the east coast of the United States, southeast Australia and New Zealand, southern Chile, northern Japan, and the Mediterranean coasts, among other. Besides the Antarctic region, PLs pose the greatest threats to the coasts of the Nordic Seas and the Gulf of Alaska. IKE's spatial distribution patterns may appear different from the LPS frequencies because IKE is storm size-sensitive. For example, even though high TC frequencies are found concentrated in the Eastern Pacific basin (Figure 8a), TC IKE is far more prominent in the Western North Pacific basin due to its largest mean observed TC size among all major basins (Chavas & Emanuel, 2010). Similarly, IKE for SS in the Mediterranean Sea appear much smaller compared to other hotspots like the Western North Pacific and the northwest Atlantic, as TLCs in an open ocean basin can be relatively larger without topographic constraints. Those larger TLCs can possibly be embedded TLCs or "twin-cyclones" like the one shown in Figure S4 in Supporting Information S1, and their existence is documented in many case studies in the two basins (e.g., Fu et al., 2018; Yamamoto, 2012; Yokoyama & Yamamoto, 2019).

Objectively tracked LPSs are often used in fractional precipitation contribution studies to tease out the contribution of each LPS type to the total precipitation (e.g., Prat & Nelson, 2013; Prein et al., 2023). The outputs from our framework could be a good source for this purpose, as precipitation blobs can be derived and labeled in a similar manner as for the size blob. Blobs (areas) that satisfy the smoothed 850 hPa cyclonic relative vorticity (CRV) threshold (CRV $> 2 \times 10^{-5}$ s^{-1}) and a minimum 3-hourly total precipitation threshold of 0.3 mm per 3 hr

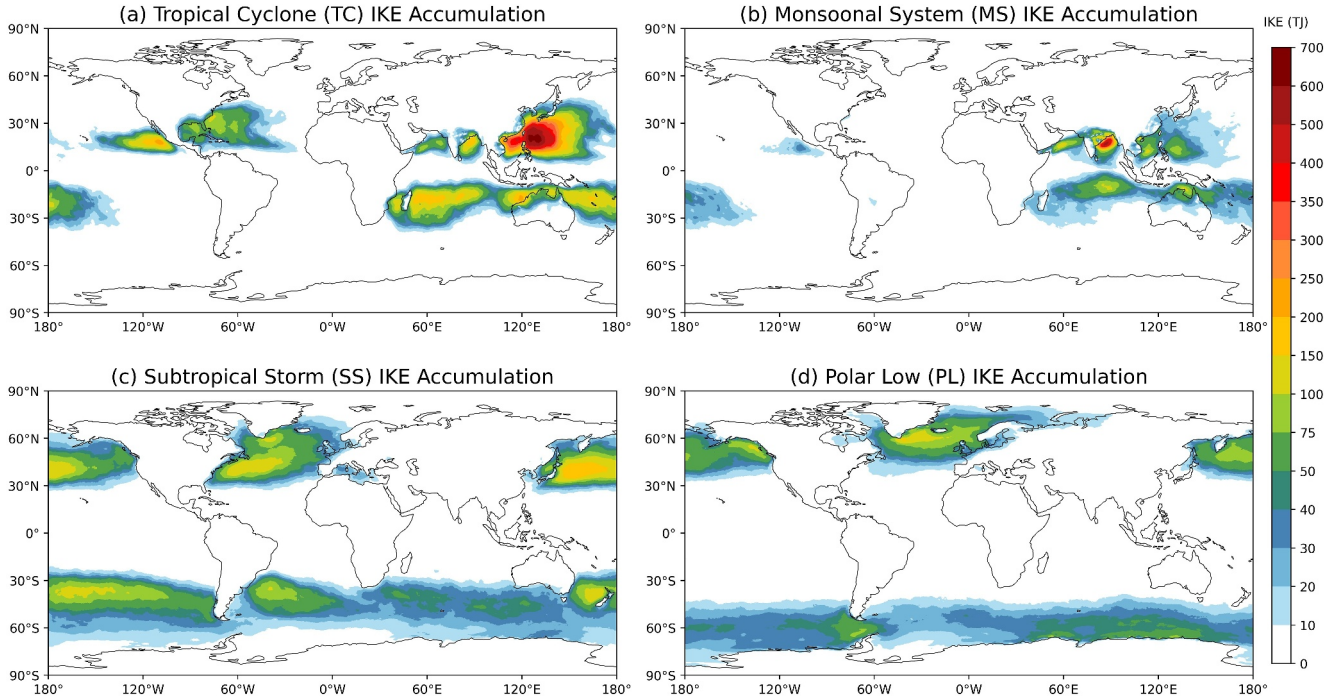

Figure 11. Integrated Kinetic Energy (IKE) of (a) tropical cyclone (TC), (b) monsoonal system (MS), (c) subtropical storm (SS), and (d) polar low (PL) accumulated over the 1979–2022 period.

(0.1 mm hr^{-1}) are highlighted as LPS-associated precipitation and tagged with LPS labels (see Figure S6 in Supporting Information S1). We consider this dynamic precipitation detection method more flexible than a fixed or uniform radius method that was often implemented in previous studies (e.g., Dare et al., 2012; Stansfield et al., 2020). We select each class of high-impact LPS nodes and their associated precipitation blobs in the same way as we do for IKE. We demonstrate the fractional contribution of precipitation from the four types of high-impact LPS nodes in Figure 12. The results suggest that TCs contribute over 40% of total precipitation along the coasts of northwestern Australia and south of Baja California. MSs are responsible for a larger fraction of total precipitation than TCs throughout South Asia and inland China. SSs make up about 5% of total precipitation along the coastal region of the Mediterranean Sea and about 6%–7% near northern Japan and the coasts along the Japan Sea. PLs are responsible for several percent of total precipitation in the United Kingdom, northern Europe, and along the coast of Alaska. Since TLCs are active in the winter season, one may expect heavy snowfall as the form of their precipitation.

7. Summary and Conclusions

In this study, we propose an all-in-one detection and classification framework which we refer to as the System for Classification of Low-Pressure Systems (SyCLoPS). In essence, SyCLoPS combines multiple specialized LPS detectors into a single framework, which has the effect of improving classification performance for individual features through a comprehensive treatment of boundary cases. SyCLoPS is developed atop the TempestExtremes (TE) software package (Ullrich, 2024; Ullrich et al., 2021; Ullrich & Zarzycki, 2017). It is tuned and subsequently applied to the ERA5 reanalysis. To the authors' best knowledge, this work represents the first attempt to classify all LPSs in a single global data set. Classification parameters and thresholds are set using conventional definitions, observations, and physical intuition, with some assistance from mathematical optimization and basic machine learning methods. To summarize, SyCLoPS performs detection and classification following two main steps: First is to detect and track LPSs spanning all intensities globally and compute the input atmospheric parameters as shown in Appendix C using TE commands. Second, a Python classifier is applied to construct the input catalog and take in the input parameters for classifying (labeling) all detected LPS nodes and tracks following the workflow shown in Figure 1. The classifier also incorporates additional information about the nodes and tracks, such as extratropical transition nodes and whether the LPS track should be considered quasi-stationary, into the final classified LPS

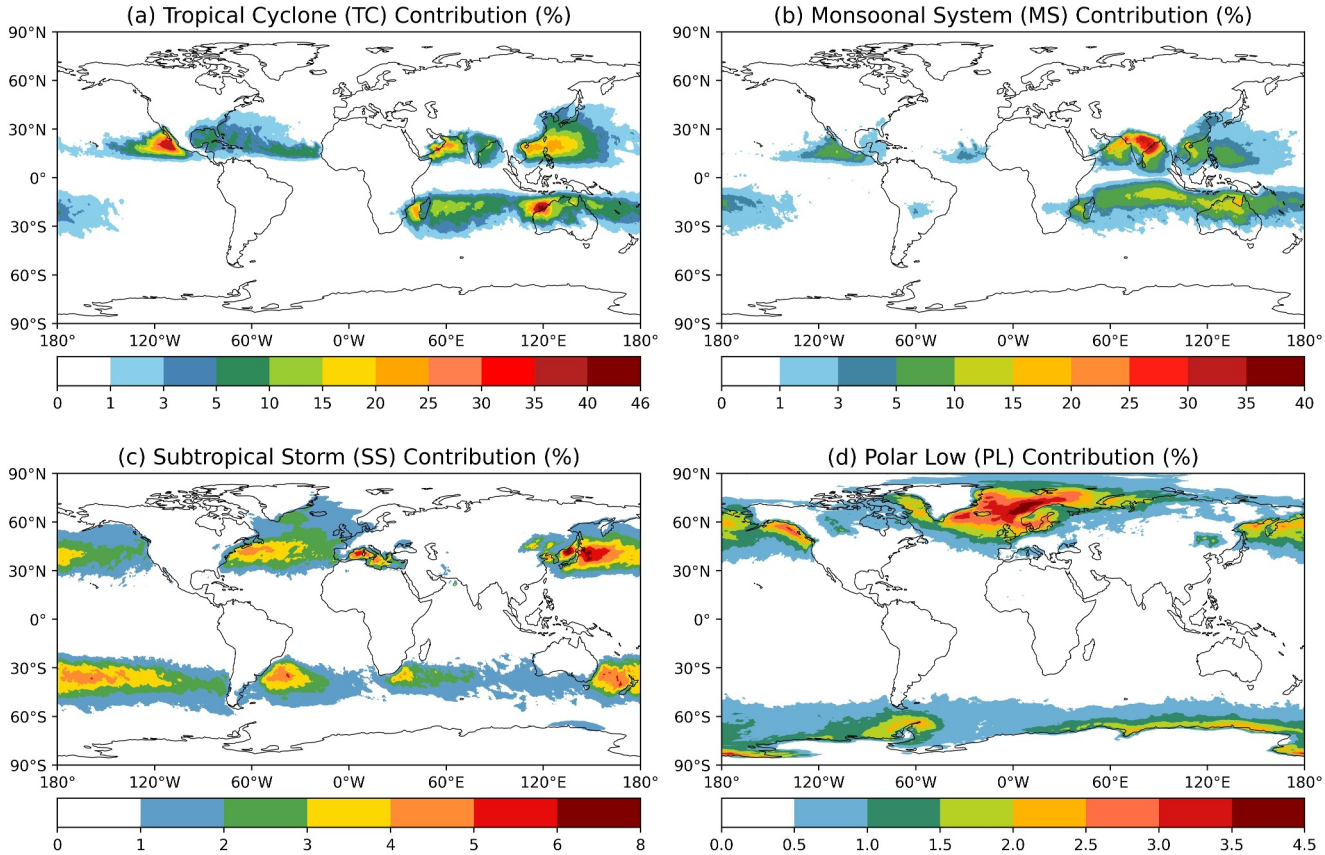

Figure 12. Fractional precipitation contributions from (a) tropical cyclone (TC), (b) monsoonal system (MS), (c) subtropical storm (SS), and (d) polar low (PL) for the 1979–2022 period.

catalog together with the LPS node and track labels. The classification process of SyCLoPS features the following novelties:

1. Because a single intuitive workflow is employed, all LPS nodes are assigned one of the 16 LPS class labels at once. No LPS node is repeated or doubly classified. Consequently, LPS phase evolution can be traced using the labeled nodes as shown in Figure 10.
2. No topographical, latitudinal, or temporal restrictions need to be applied in order to use this framework, and the detection threshold is low enough to include very weak LPS nodes in the detected LPS tracks. As a result, a much more complete LPS lifecycle can be obtained for each LPS track.
3. To address the insufficiency of using warm-core criteria to disentangle tropical systems, SyCLoPS proposes a new way to objectively and physically define tropical and non-tropical systems using 100 hPa level relative humidity and large-scale deep-layer wind shear.
4. SyCLoPS features the first global TLC (subtropical storms and polar lows) detection scheme by detecting similar physical features to tropical cyclones among non-tropical system candidates.

Using the LPS track labels in the classified catalog, our results show that the unified framework improves upon the previously reported best TC detection skill with TE (Bourdin et al., 2022; Zarzycki & Ullrich, 2017) by both increasing HR and lowering FAR. We found that the lowered FAR is mainly contributed by successfully identifying subtropical storms in the subtropics. Detection skill for MS is comparable to previous work (Vishnu et al., 2020). Upon comparing the labels given by SyCLoPS to the corresponding IBTrACS labels, we observe that SyCLoPS can reasonably label the LPS status in different stages of a TC. We also demonstrate that the resulting classified catalog can be used to study the evolution, annual frequencies, vertical cross-section composites, IKE accumulation, and fractional precipitation contribution of each LPS class. These potential applications are useful

for general LPS studies, and it could be valuable if applied to climate model outputs to investigate the trends of LPS activities under the effects of climate change. SyCLoPS may also be applicable in real-time operations and weather model outputs. Furthermore, information in the classified catalog may be used as data labels to train a machine learning model. We intend to pursue additional research tasks on those topics using SyCLoPS.

Users may also personalize the framework to meet their own needs with the data and codes provided in SyCLoPS. For example, the detection procedure for a single type of LPS in a given data set can be easily isolated following a single path from the workflow. Users may also modify the TE specifications to optimize detection for a specific type of LPS (in a specific region) like the one we show Text S7 in Supporting Information S1. More LPS sub-classes may be derived from SyCLoPS catalogs and the detection of other atmospheric features. For example, weaker tropical LPSs may be separated into different classes by matching them to distinct tropical waves in the lower troposphere, and TLCs may be divided into those that develop in a front-shear environment versus a reverse-shear environment.

There are some notable limitations in SyCLoPS. Firstly, SyCLoPS is based upon ERA5 data set, so the thresholds and parameter choices could be biased if applied directly to another global or regional data set. While we have proposed some suggestions that would allow SyCLoPS to adapt to different data sets, and have shown in Appendix B that SyCLoPS's performance is stable across different adaptation experiments, more fine-tuning in the detection and classification processes may be required. It should also be noted that a data set with a resolution coarser than ERA5 may be insufficient for detection and classification of smaller features such as early-stage TCs and TLCs. Second, although SyCLoPS features detection and classification of LPSs over any terrain, signals in MSLP or any low-level atmospheric fields can be distorted by elevated or rough topography. Detection over or near those regions are subject to greater errors, especially for weak systems. Third, ultimately, the hard cut-off threshold we impose between LPS phases is somewhat arbitrary: namely, there is always a gray zone or transition zone when it comes to the thresholds for a given LPS. Nonetheless, objective LPS detection and classification reduces biases introduced by human error and subjectivity because an objective standard can be strictly followed. However, by nature an LPS can exist in an "impure" and somewhat ambiguous state, which is contrary to fixed thresholds. This conflict is most obvious when a detected LPS persists at the edge of our defined thresholds, leading to its classification jumping between two labels. And lastly, confidence in detecting and classifying global TLC systems is still low due to a lack of global observations. The method for calculating LPS size in TE as described in Appendix E for classifying TLCs can be further improved to more accurately represent the size of a smaller TLC in a larger circulation or the background flow. We expect that there will be other deficiencies discovered and questions raised in the practical use of this experimental framework. Hence, we aim to address the remaining issues and evolve the algorithms for future versions of this framework.

Appendix A: Variables Used in SyCLoPS

Table A1

Additionally, 10-m U and V-component Wind (VAR_10U and VAR_10V) are used to calculate the maximum surface wind speed (WS) of an LPS as a reference information in the classified catalog. It does not play a role in the detection and classification process.

Although SyCLoPS is tested on 3-hourly data, as suggested in Appendix B below, it's possible to use 6-hourly data or even lower frequency data for parameters that change more slowly and smoothly. The recommended TE commands for implementing a 6-hourly frequency detection under SyCLoPS framework are included Text S6 in Supporting Information S1.

Table A1
Default ERA5 Variables Used in SyCLoPS for Detection and Classification

Variable name	Pressure level (hPa)
U-component Wind (U)	925, 850, 200[c]
V-component Wind (V)	925, 850, 200[c]
Temperature (T)	850
Relative Humidity (R)[a]	850, 100
Mean Sea Level Pressure (MSL)	Sea Level
Geopotential (Z)	Surface, 925, 700, 500, 300[c]
Relative Vorticity (VO)[b]	500

[a]Specific humidity can be converted to R with additional temperature information. [b]VO can also be computed by U and V if not directly available. [c]These default levels can be replaced by 250 hPa. See Appendix B for details.

Appendix B: Experiments for Climate Model Data Adaptations

Four adaptation experiments are performed on SyCLoPS to test how SyCLoPS can be adapted to a typical high-resolution climate model output. In

these high-resolution models (e.g., those in the HighresMIP submission), RH at 100 hPa is usually only available in daily frequency, so our first experiment resamples ERA5 3-hourly RH data to daily frequency (daily-mean) and recalculates RH100MAX for classification (i.e., each grid point will have the same RHMAX100 for 8 3-hourly time steps in a day). Most climate models only output 6-hourly frequency (instead of 3) for many of the fields we use in SyCLoPS. Therefore, the second experiment resamples the 3-hourly frequency input catalog of SyCLoPS to 6-hourly frequency (similar to using a 6-hourly detection rate) before performing the same classification. In addition, the number of nodes (time steps) needed to satisfy the TC, MS, SS and PL track conditions is halved to reflect the frequency change. For example, 4 TC nodes (instead of 8) in a track are required for the TC track condition under 6-hourly frequency data.

Finally, some climate model outputs only have 250 hPa data instead of the 200 hPa data (used in DEEPSHEAR and WS200PMX) or 300 hPa data (used in UPPTKCC) we use in SyCLoPS. Therefore, the third experiment opts to use 250 hPa data in ERA5 and the subsequent adjustments to the classification conditions are needed to achieve the optimal detection skills (or to match our original definition to justify the polar jet/front):

1. In the tropical condition, the DEEPSHEAR threshold is changed to: DEEPSHEAR < 13 m s^{-1}
2. TC Condition is changed to: MSLPCC20 > 225 Pa, LOWTKCC < 0 m^2 s^{-2} and UPPTKCC < -147 m^2 s^{-2}.
3. TC Track Condition is changed: At least 6 3-hourly TC-labeled nodes in a track are required to satisfy the TC Track Condition.
4. WS200PMX should be renamed to WS250PMX with the following changes: In the SC condition, use WS250PMX > 35 m s^{-1}. And to separate SS and PL, use WS250PMX > 30 m s^{-1}

The results of these adaptation experiments are summarized in Table B1 below. As shown, the detection skills and labeling accuracy of the three adaptation experiments are generally very similar to the original algorithm, suggesting the flexibility of SyCLoPS in adapting to climate model data. It's also not surprising that the TLC detection skill degrades more noticeably at a lower sampling frequency in the 6-hourly data frequency experiment given that many TLCs are transient.

Table B1
Adaptation Experiment Performance

Method	TC detection	Label accuracy	MS detection	TLC detection
Original	HR = 78.2%	TS: 96.6%	CSI = 0.83	HR ≈ 80%
	FAR = 14.6%	TC: 74%		
	HRMFAR = 63.6%	EX: 78%		IR = 11.9%
Daily-mean RH100MAX	HR = 78.0%	TS: 96.6%	CSI = 0.83	HR ≈ 80%
	FAR = 14.7%	TC: 74%		IR = 11.7%
	HRMFAR = 63.3%	EX: 79%		
6-hourly Frequency	HR = 78.4%	TS: 96.6%	CSI = 0.82	HR ≈ 70%
	FAR = 15.2%	TC: 75%		IR = 14.8%
	HRMFAR = 63.2%	EX: 78%		
250 hPa Parameters	HR = 78.7%	TS: 96.3%	CSI = 0.83	HR ≈ 80%
	FAR = 15.1%	TC: 72%		IR = 11.6%
	HRMFAR = 63.6%	EX: 84%		

Appendix C: Catalog Column Table

Table C1

Table C1
Column Table for the Input Catalog (Top) and Classified Catalog (Bottom)

Column	Unit	Description
TID	–	LPS track ID (0-based) in both the input and classified catalog
ISOTIME	–	UTC timestamp (ISO time) of the LPS node in both catalogs
LAT	°	Latitude of the LPS node in both catalogs
LON	°	Longitude of the LPS node in both catalogs
MSLP	Pa	Mean sea level pressure at the LPS node in both catalogs
MSLPCC20	Pa	Greatest positive closed contour delta of MSLP over a 2.0° GCD (the core of an LPS)
MSLPCC55	Pa	Greatest positive closed contour delta of MSLP over a 5.5° GCD
DEEPSHEAR	$m\ s^{-1}$	Average deep-layer wind speed shear between 200 hPa and 850 hPa over a 10.0° GCD
UPPTKCC	$m^2\ s^{-2}$	Greatest negative closed contour delta of the upper-level thickness between 300 hPa and 500 hPa over a 6.5° GCD, referenced to the maximum value within 1.0° GCD
MIDTKCC	$m^2\ s^{-2}$	Greatest negative closed contour delta of the middle-level thickness between 500 hPa and 700 hPa over a 3.5° GCD, referenced to the maximum value within 1.0° GCD
LOWTKCC[a]	$m^2\ s^{-2}$	Greatest negative closed contour delta of the lower-level thickness between 700 hPa and 925 hPa over a 3.5° GCD, referenced to the maximum value within 1.0° GCD
Z500CC	$m^2\ s^{-2}$	Greatest positive closed contour delta of geopotential at 500 hPa over a 3.5° GCD referenced to the minimum value within 1.0° GCD
VO500AVG	s^{-1}	Average relative vorticity over a 2.5° GCD
RH100MAX	%	Maximum relative humidity at 100 hPa within 2.5° GCD
RH850AVG	%	Average relative humidity over a 2.5° GCD at 850 hPa
T850	K	Air temperature at 850 hPa at the LPS node
Z850	$m^2\ s^{-2}$	Geopotential at 850 hPa at the LPS node
ZS	$m^2\ s^{-2}$	Geopotential at the surface at the LPS node
U850DIFF	$m\ s^{-1}$ sr	Difference between the weighted area mean of positive and negative values of 850 hPa U-component wind over a 5.5° GCD
WS200PMX	$m\ s^{-1}$	Maximum poleward value of 200 hPa wind speed within 1.0° GCD longitude
RAWAREA	km^2	The raw defined size (see Appendix E) of the LPS
LPSAREA	km^2	The adjusted defined size of the LPS in both catalogs
WS	$m\ s^{-1}$	Maximum wind speed at the 10-m level within 2.0° GCD
Full_Name	–	The full LPS name based on the classification
Short_Label	–	The assigned LPS label (the abbreviation of the full name)
Tropical_Flag	–	1 if the LPS is designated as a tropical system, otherwise 0
Transition_Zone	–	1 if the LPS is in the defined transition zone, otherwise 0
Track_Info	–	"TC," "MS," "SS(STLC)," "PL(PTLC)," "QS" denoted for TC, MS, SS, PL and QS tracks; "EXT," "TT" denoted for extratropical and tropical transition completion nodes
IKE	TJ	The integrated kinetic energy computed based on the LPS size blobs that are used to define RAWAREA

[a]925 hPa may be replaced by 850 hPa if data at this level is unavailable in some data sets.

Appendix D: Condition List

Table D1

Table D1
Classification Conditions

Condition name	Conditions
High-altitude Condition[a]	Z850 > ZS
Dryness Condition	RH850AVG < 60%
Cyclonic Condition	VO500AVG ≥ (<) 0 s^{-1} if LAT ≥ (<) 0°
Tropical Condition	RH100MAX > 20%; DEEPSHEAR < 18 m s^{-1}; T850 > 280 K
Transition Condition	Tropical Condition = True; DEEPSHEAR > 10 m s^{-1} or RH100MAX < 55%
TC Condition	MSLPCC20 > 215 Pa; LOWTKCC < 0 m^2 s^{-2}; UPPTKCC < −107.8 m^2 s^{-2}
TD Condition	MSLPCC55 > 160 Pa; UPPTKCC < 0 m^2 s^{-2}
MS Condition	U850DIFF > 0 m s^{-1}; RH850AVG > 85%
TLC Condition[b]	MSLPCC20 > 190 Pa; LOWTKCC and MIDTKCC < 0 m^2 s^{-2}; (LPSAREA < 5.5 × 10^5 km^2; LPSAREA > 0 km^2) or (MSLPCC20 > 420 Pa; MSLPCC20: MSLPCC55 > 0.5)
SC Condition	LOWTKCC < 0 m^2 s^{-2}; Z500CC > 0 m^2 s^{-2}; WS200PMX[c] > 30 m s^{-1}
TC Track Condition	At least 8 (8+) 3-hourly TC-labeled nodes in an LPS track
MS Track Condition	10+ 3-hourly "TLO(ML)" or "TD(MD)"-labeled nodes in an LPS track
SS Track Condition	2+ 3-hourly TLC-labeled nodes ("SS(STLC)" or "PL(PTLC)") and 1 "SS(STLC)"-labeled node in an LPS track
PL Track Condition	2+ 3-hourly TLC-labeled nodes ("SS(STLC)" or "PL(PTLC)") and 1 "PL(PTLC)"-labeled node in an LPS track
QS Track Condition	See Text S3 in Supporting Information S1 for details

[a]It can be simply checking Z850 data availability (null or not) in some data sets. [b]See Section 5.3 for a potential alternative. [c]WS200PMX criteria used in this framework may be supplemented by other parameters in some regional models. See Text S4 in Supporting Information S1 for details.

Appendix E: LPSAREA Computation

To calculate LPS size, we refer to the definition of TC size which is typically determined by a TC's outer surface wind radius. We first use TE to detect blobs (areas) of smoothed 850 hPa cyclonic relative vorticity (CRV) > 2 × 10^{-5} s^{-1} and 925 hPa wind speed > 12 m s^{-1}. An alternative condition to this detection requirement is CRV > 4 × 10^{-5} s^{-1} so that TC eyes and EXs' central weaker wind areas can be captured. Wind speed from 925 hPa is used for this calculation, for it is a commonly found lower model level above the surface level. Surface level winds are not used since they can be greatly distorted by complex topography. The 12 m s^{-1} threshold is obtained using a log wind profile from the 8 or 9 m s^{-1} surface outer wind speed threshold often found in TC-size-related studies using ERA5 or climate models (e.g., Bian et al., 2021; Stansfield et al., 2020). The smoothed CRV field is used to control the boundary of an LPS so that the outer wind fields are less likely to connect with an unrelated system nearby. Each detected size blob is then assigned to a detected LPS node if the node is within 5° GCD of the centroid of the blob at the same timestamp, or otherwise within the region bounded by the minimum/maximum latitude/longitude (extent) of the blob. Information on the centroid, extent, and size (area) of each blob can be directly output by TE. If multiple nodes are found for one blob, the blob is assigned to the node with the lowest MSLP. Next, the areas of all the blobs paired with each node are added together as raw LPS sizes (areas). To avoid misclassifying EXs/SCs as TLCs near shorelines with elevated topography, we adjust the raw LPS size if the LPS is close to those shorelines with its wind field largely affected by topography. Specifically, we multiply the raw LPS size by 2 if only 30%–70% of surface geopotential within 5° GCD of an LPS is smaller than 7,000 m^2 s^{-2} (approximately the 925 hPa level). This adjusted LPS size is defined as LPSAREA (in km^2). For a quick comparison, the sizes of 2010–2021 Western North Pacific TCs computed by our method and the sizes given by the Japan Meteorological Agency in IBTrACS have a reasonably high correlation coefficient of 0.63, with very

high statistical significance. Furthermore, the average and median global PL size (in radius) given by LPSAREA is 231 and 206 km which are very close to the 221 and 200 km suggested by the PL radius records in the STARS data set. The non-adjusted (raw) LPS size computed by this method is included as the "RAWAREA" column in the input catalog. The TE commands for computing the LPSAREA parameter are printed Text S6 in Supporting Information S1.

Data Availability Statement

The latest version (version 2.2.3) of TempestExtremes (TE) can be accessed from https://doi.org/10.5281/zenodo.13830377 (Ullrich, 2024). The input and the classified catalog created in this study, the shell script for TE commands, the Python Classifier and a user manual are all available via the Zenodo repository (Han & Ullrich, 2024) at https://doi.org/10.5281/zenodo.10906284. We aim to keep updating this online data set to reflect new improvements. The ERA5 data set was obtained from the Research Data Archive (European Centere for Medium-Range Weather Forecasts, 2019) at the National Center for Atmospheric Research (https://doi.org/10.5065/BH6N-5N20). The IBTrACS archive (Knapp et al., 2018) can be retrieved from https://www.ncei.noaa.gov/products/international-best-track-archive. The STARS polar low list (Noer et al., 2011) is available at: https://projects.met.no/polarlow/stars-dat. The following two websites were used to evaluate the status of tracked Mediterranean cyclones: https://meteorologia.uib.eu/medicanes/medicanes_list.html maintained by the meteorology group of the University of the Balearic Islandsor and http://medicanes.altervista.org run by Daniele Bianchino. The objectively tracked easterly wave data set is downloaded from https://doi.org/10.17605/OSF.IO/J4HPQ published by Lawton and Majumdar (2018).

Acknowledgments

This work is supported by the Program for Climate Model Diagnosis and Intercomparison (PCMDI) under the auspices of the U.S. Department of Energy at Lawrence Livermore National Laboratory under contract DE-AC52-07NA27344. The authors thank Colin Zarzycki, Kevin Reed, and Haoyu Zhuang for helpful discussion and feedback. The authors thank S. Vishnu for providing the electronic version of the Sikka archive converted by Sarah Ditchek. The authors thank Emmanouil Flaounas for sharing the subjectively tracked Mediterranean cyclone data. The authors are also very grateful for the thorough and constructive comments from Malcolm Roberts and Alice Miller and two other anonymous reviewers.

References

Bernhardt, J. E., & DeGaetano, A. T. (2012). Meteorological factors affecting the speed of movement and related impacts of extratropical cyclones along the US East Coast. *Natural Hazards*, *61*(3), 1463–1472. https://doi.org/10.1007/s11069-011-0078-0

Bian, G.-F., Nie, G.-Z., & Qiu, X. (2021). How well is outer tropical cyclone size represented in the era5 reanalysis dataset? *Atmospheric Research*, *249*, 105339. https://doi.org/10.1016/j.atmosres.2020.105339

Blackmon, M. L., Wallace, J. M., Lau, N.-C., & Mullen, S. L. (1977). An observational study of the northern hemisphere wintertime circulation. *Journal of the Atmospheric Sciences*, *34*(7), 1040–1053. https://doi.org/10.1175/1520-0469(1977)034<1040:aosotn>2.0.co;2

Bourdin, S., Fromang, S., Dulac, W., Cattiaux, J., & Chauvin, F. (2022). Intercomparison of four algorithms for detecting tropical cyclones using era5. *Geoscientific Model Development*, *15*(17), 6759–6786. https://doi.org/10.5194/gmd-15-6759-2022

Cavicchia, L., Dowdy, A., & Walsh, K. (2018). Energetics and dynamics of subtropical Australian east coast cyclones: Two contrasting cases. *Monthly Weather Review*, *146*(5), 1511–1525. https://doi.org/10.1175/mwr-d-17-0316.1

Chavas, D. R., & Emanuel, K. A. (2010). A quikscat climatology of tropical cyclone size. *Geophysical Research Letters*, *37*(18). https://doi.org/10.1029/2010gl044558

Dare, R. A., Davidson, N. E., & McBride, J. L. (2012). Tropical cyclone contribution to rainfall over Australia. *Monthly Weather Review*, *140*(11), 3606–3619. https://doi.org/10.1175/mwr-d-11-00340.1

Datt, I., Camargo, S. J., Sobel, A. H., McTAGGART-COWAN, R., & Wang, Z. (2022). An investigation of tropical cyclone development pathways as an indicator of extratropical transition. *Journal of the Meteorological Society of Japan. Ser. II*, *100*(4), 707–724. https://doi.org/10.2151/jmsj.2022-037

Doran, P. T., Priscu, J. C., Lyons, W. B., Walsh, J. E., Fountain, A. G., McKnight, D. M., et al. (2002). Antarctic climate cooling and terrestrial ecosystem response. *Nature*, *415*(6871), 517–520. https://doi.org/10.1038/nature710

Emanuel, K. (2005). Genesis and maintenance of mediterranean hurricanes. *Advances in Geosciences*, *2*, 217–220. https://doi.org/10.5194/adgeo-2-217-2005

European Centre for Medium-Range Weather Forecasts. (2019). Research data archive at the national center for atmospheric research, computational and information systems laboratory [Dataset]. https://doi.org/10.5065/BH6N-5N20

Evans, J. L., & Braun, A. (2012). A climatology of subtropical cyclones in the south Atlantic. *Journal of Climate*, *25*(21), 7328–7340. https://doi.org/10.1175/jcli-d-11-00212.1

Feng, X., Liu, C., Fan, G., Liu, X., & Feng, C. (2016). Climatology and structures of southwest vortices in the NCEP climate forecast system reanalysis. *Journal of Climate*, *29*(21), 7675–7701. https://doi.org/10.1175/jcli-d-15-0813.1

Fita, L., Romero, R., Luque, A., Emanuel, K., & Ramis, C. (2007). Analysis of the environments of seven mediterranean tropical-like storms using an axisymmetric, nonhydrostatic, cloud resolving model. *Natural Hazards and Earth System Sciences*, *7*(1), 41–56. https://doi.org/10.5194/nhess-7-41-2007

Flaounas, E., Aragão, L., Bernini, L., Dafis, S., Doiteau, B., Flocas, H., et al. (2023). A composite approach to produce reference datasets for extratropical cyclone tracks: Application to mediterranean cyclones. *Weather and Climate Dynamics*, *4*(3), 639–661. https://doi.org/10.5194/wcd-4-639-2023

Flaounas, E., Davolio, S., Raveh-Rubin, S., Pantillon, F., Miglietta, M. M., Gaertner, M. A., et al. (2022). Mediterranean cyclones: Current knowledge and open questions on dynamics, prediction, climatology and impacts. *Weather and Climate Dynamics*, *3*(1), 173–208. https://doi.org/10.5194/wcd-3-173-2022

Fu, S.-M., Sun, J.-H., Li, W.-L., & Zhang, Y.-C. (2018). Investigating the mechanisms associated with the evolutions of twin extratropical cyclones over the northwest Pacific Ocean in mid-January 2011. *Journal of Geophysical Research: Atmospheres*, *123*(8), 4088–4109. https://doi.org/10.1002/2017jd027852

Gan, M. A., Kousky, V. E., & Ropelewski, C. F. (2004). The south America monsoon circulation and its relationship to rainfall over west-central Brazil. *Journal of Climate*, *17*(1), 47–66. https://doi.org/10.1175/1520-0442(2004)017<0047:tsamca>2.0.co;2

Garde, L. A., Pezza, A. B., & Bye, J. A. T. (2010). Tropical transition of the 2001 Australian duck. *Monthly Weather Review*, *138*(6), 2038–2057. https://doi.org/10.1175/2009mwr3220.1

Gozzo, L. F., da Rocha, R. P., Reboita, M. S., & Sugahara, S. (2014). Subtropical cyclones over the southwestern south Atlantic: Climatological aspects and case study. *Journal of Climate*, *27*(22), 8543–8562. https://doi.org/10.1175/jcli-d-14-00149.1

Guishard, M. P., Evans, J. L., & Hart, R. E. (2009). Atlantic subtropical storms. Part II: Climatology. *Journal of Climate*, *22*(13), 3574–3594. https://doi.org/10.1175/2008jcli2346.1

Han, Y., & Ullrich, P. A. (2024). The system for classification of low-pressure systems (syclops) dataset (based on era5) [Dataset]. *Zenodo*. https://doi.org/10.5281/zenodo.10906284

Hart, R. E. (2003). A cyclone phase space derived from thermal wind and thermal asymmetry. *Monthly Weather Review*, *131*(4), 585–616. https://doi.org/10.1175/1520-0493(2003)131<0585:acpsdf>2.0.co;2

Heo, K.-Y., & Ha, K.-J. (2008). Snowstorm over the southwestern coast of the Korean peninsula associated with the development of mesocyclone over the yellow sea. *Advances in Atmospheric Sciences*, *25*(5), 765–777. https://doi.org/10.1007/s00376-008-0765-2

Hepworth, E., Messori, G., & Vichi, M. (2022). Association between extreme atmospheric anomalies over Antarctic sea ice, southern ocean polar cyclones and atmospheric rivers. *Journal of Geophysical Research: Atmospheres*, *127*(7), e2021JD036121. https://doi.org/10.1029/2021jd036121

Hersbach, H., Bell, B., Berrisford, P., Hirahara, S., Horányi, A., Muñoz-Sabater, J., et al. (2020). The era5 global reanalysis. *Quarterly Journal of the Royal Meteorological Society*, *146*(730), 1999–2049. https://doi.org/10.1002/qj.3803

Hodges, K., Cobb, A., & Vidale, P. L. (2017). How well are tropical cyclones represented in reanalysis datasets? *Journal of Climate*, *30*(14), 5243–5264. https://doi.org/10.1175/jcli-d-16-0557.1

Hodges, K. I. (1994). A general method for tracking analysis and its application to meteorological data. *Monthly Weather Review*, *122*(11), 2573–2586. https://doi.org/10.1175/1520-0493(1994)122<2573:agmfta>2.0.co;2

Hoinka, K. P., & Castro, M. D. (2003). The Iberian Peninsula thermal low. *Quarterly Journal of the Royal Meteorological Society: A journal of the atmospheric sciences, applied meteorology and physical oceanography*, *129*(590), 1491–1511. https://doi.org/10.1256/qj.01.189

Holland, G. J., Lynch, A. H., & Leslie, L. M. (1987). Australian east-coast cyclones. Part I: Synoptic overview and case study. *Monthly Weather Review*, *115*(12), 3024–3036. https://doi.org/10.1175/1520-0493(1987)115<3024:aeccpi>2.0.co;2

Hopsch, S. B., Thorncroft, C. D., & Tyle, K. R. (2010). Analysis of African easterly wave structures and their role in influencing tropical cyclogenesis. *Monthly Weather Review*, *138*(4), 1399–1419. https://doi.org/10.1175/2009mwr2760.1

Hunt, K. M., Turner, A. G., Inness, P. M., Parker, D. E., & Levine, R. C. (2016). On the structure and dynamics of Indian monsoon depressions. *Monthly Weather Review*, *144*(9), 3391–3416. https://doi.org/10.1175/mwr-d-15-0138.1

Hurley, J. V., & Boos, W. R. (2015). A global climatology of monsoon low-pressure systems. *Quarterly Journal of the Royal Meteorological Society*, *141*(689), 1049–1064. https://doi.org/10.1002/qj.2447

Iwao, K., Inatsu, M., & Kimoto, M. (2012). Recent changes in explosively developing extratropical cyclones over the winter northwestern Pacific. *Journal of Climate*, *25*(20), 7282–7296. https://doi.org/10.1175/jcli-d-11-00373.1

Knapp, K. R., Diamond, H. J., Kossin, J. P., Kruk, M. C., & Schreck, C. J. (2018). International best track archive for climate stewardship (IBTrACS) project, version 4 [Dataset]. *NOAA National Centers for Environmental Information*. https://doi.org/10.25921/82ty-9e16

Knapp, K. R., Kruk, M. C., Levinson, D. H., Diamond, H. J., & Neumann, C. J. (2010). The international best track archive for climate stewardship (IBTrACS) unifying tropical cyclone data. *Bulletin of the American Meteorological Society*, *91*(3), 363–376. https://doi.org/10.1175/2009bams2755.1

Koch, P., Wernli, H., & Davies, H. C. (2006). An event-based jet-stream climatology and typology. *International Journal of Climatology: A Journal of the Royal Meteorological Society*, *26*(3), 283–301. https://doi.org/10.1002/joc.1255

Kreussler, P., Caron, L.-P., Wild, S., Loosveldt Tomas, S., Chauvin, F., Moine, M.-P., et al. (2021). Tropical cyclone integrated kinetic energy in an ensemble of highresmip simulations. *Geophysical Research Letters*, *48*(5), e2020GL090963. https://doi.org/10.1029/2020gl090963

Landsea, C. W., & Franklin, J. L. (2013). Atlantic hurricane database uncertainty and presentation of a new database format. *Monthly Weather Review*, *141*(10), 3576–3592. https://doi.org/10.1175/mwr-d-12-00254.1

Lau, W. K., & Kim, K.-M. (2015). Robust Hadley circulation changes and increasing global dryness due to CO_2 warming from CMIP5 model projections. *Proceedings of the National Academy of Sciences*, *112*(12), 3630–3635. https://doi.org/10.1073/pnas.1418682112

Lavaysse, C., Flamant, C., Janicot, S., Parker, D. J., Lafore, J.-P., Sultan, B., & Pelon, J. (2009). Seasonal evolution of the west African heat low: A climatological perspective. *Climate Dynamics*, *33*(2–3), 313–330. https://doi.org/10.1007/s00382-009-0553-4

Lawton, Q., & Majumdar, S. (2018). Objective tracking of African easterly waves in reanalysis data (updated through 2022) [Dataset]. *OSF*. https://doi.org/10.17605/OSF.IO/J4HPQ

Lawton, Q. A., Majumdar, S. J., Dotterer, K., Thorncroft, C., & Schreck, C. J., III. (2022). The influence of convectively coupled kelvin waves on African easterly waves in a wave-following framework. *Monthly Weather Review*, *150*(8), 2055–2072. https://doi.org/10.1175/mwr-d-21-0321.1

Li, J., & Zeng, Q. (2003). A new monsoon index and the geographical distribution of the global monsoons. *Advances in Atmospheric Sciences*, *20*(2), 299–302. https://doi.org/10.1007/s00376-003-0016-5

Li, L., Zhang, R., Wen, M., Duan, J., & Qi, Y. (2019). Characteristics of the Tibetan plateau vortices and the related large-scale circulations causing different precipitation intensity. *Theoretical and Applied Climatology*, *138*(1–2), 849–860. https://doi.org/10.1007/s00704-019-02870-4

Lodise, J., Merrifield, S., Collins, C., Rogowski, P., Behrens, J., & Terrill, E. (2022). Global climatology of extratropical cyclones from a new tracking approach and associated wave heights from satellite radar altimeter. *Journal of Geophysical Research: Oceans*, *127*(11), e2022JC018925. https://doi.org/10.1029/2022jc018925

Lu, J., & Ding, Y. (1989). Climatic study on the summer tropical easterly jet at 200 hPa. *Advances in Atmospheric Sciences*, *6*(2), 215–226. https://doi.org/10.1007/bf02658017

Lu, J., Vecchi, G. A., & Reichler, T. (2007). Expansion of the Hadley cell under global warming. *Geophysical Research Letters*, *34*(6). https://doi.org/10.1029/2006gl028443

Masson-Delmotte, V., Zhai, P., Pirani, S., Connors, C., Péan, S., Berger, N., et al. (2021). IPCC, 2021: Summary for policymakers. In *Climate change 2021: The physical science basis. contribution of working group I to the sixth assessment report of the intergovernmental panel on climate change*.

Merlis, T. M., Cheng, K.-Y., Guendelman, I., Harris, L., Bretherton, C. S., Bolot, M., et al. (2024). Climate sensitivity and relative humidity changes in global storm-resolving model simulations of climate change. *Science Advances*, *10*(26), eadn5217. https://doi.org/10.1126/sciadv.adn5217

Montgomery, M. T., & Farrell, B. F. (1992). Polar low dynamics. *Journal of the Atmospheric Sciences*, *49*(24), 2484–2505. https://doi.org/10.1175/1520-0469(1992)049<2484:pld>2.0.co;2

National Hurricane Center. (n.d.). Glossary of NHC terms. National Hurricane Center and Central Pacific Hurricane Center. https://www.nhc.noaa.gov/aboutgloss.shtml

Neu, U., Akperov, M. G., Bellenbaum, N., Benestad, R., Blender, R., Caballero, R., et al. (2013). IMILAST: A community effort to intercompare extratropical cyclone detection and tracking algorithms. *Bulletin of the American Meteorological Society*, *94*(4), 529–547. https://doi.org/10.1175/bams-d-11-00154.1

Noer, G., Saetra, Ø., Lien, T., & Gusdal, Y. (2011). A climatological study of polar lows in the Nordic seas. *Quarterly Journal of the Royal Meteorological Society*, *137*(660), 1762–1772. https://doi.org/10.1002/qj.846

Nordeng, T. E., & Rasmussen, E. A. (1992). A most beautiful polar low. A case study of a polar low development in the bear island region. *Tellus*, *44*(2), 81–99. https://doi.org/10.1034/j.1600-0870.1992.00001.x

Oliva, M., Navarro, F., Hrbáček, F., Hernandéz, A., Nỳvlt, D., Pereira, P., et al. (2017). Recent regional climate cooling on the Antarctic Peninsula and associated impacts on the cryosphere. *Science of the Total Environment*, *580*, 210–223. https://doi.org/10.1016/j.scitotenv.2016.12.030

Poveda, G., Jaramillo, L., & Vallejo, L. F. (2014). Seasonal precipitation patterns along pathways of south American low-level jets and aerial rivers. *Water Resources Research*, *50*(1), 98–118. https://doi.org/10.1002/2013wr014087

Powell, M. D., & Reinhold, T. A. (2007). Tropical cyclone destructive potential by integrated kinetic energy. *Bulletin of the American Meteorological Society*, *88*(4), 513–526. https://doi.org/10.1175/bams-88-4-513

Prat, O. P., & Nelson, B. R. (2013). Mapping the world's tropical cyclone rainfall contribution over land using the TRMM Multi-satellite Precipitation Analysis. *Water Resources Research*, *49*(11), 7236–7254. https://doi.org/10.1002/wrcr.20527

Prein, A. F., Mooney, P. A., & Done, J. M. (2023). The multi-scale interactions of atmospheric phenomenon in mean and extreme precipitation. *Earth's Future*, *11*(11), e2023EF003534. https://doi.org/10.1029/2023ef003534

Pytharoulis, I., Craig, G. C., & Ballard, S. P. (2000). The hurricane-like mediterranean cyclone of January 1995. *Meteorological Applications: A journal of forecasting, practical applications, training techniques and modelling*, *7*(3), 261–279. https://doi.org/10.1017/s1350482700001511

Qian, W., & Lee, D.-K. (2000). Seasonal march of Asian summer monsoon. *International Journal of Climatology: A Journal of the Royal Meteorological Society*, *20*(11), 1371–1386. https://doi.org/10.1002/1097-0088(200009)20:11<1371::aid-joc538>3.0.co;2-v

Rasmussen, E. A., & Turner, J. (2003). *Mesoscale weather systems in the polar regions*. Cambridge University Press.

Reed, R. J., Norquist, D. C., & Recker, E. E. (1977). The structure and properties of African wave disturbances as observed during phase III of gate. *Monthly Weather Review*, *105*(3), 317–333. https://doi.org/10.1175/1520-0493(1977)105<0317:tsapoa>2.0.co;2

Reeder, M. J., Smith, R. K., Deslandes, R., Tapper, N. J., & Mills, G. A. (2000). Subtropical fronts observed during the 1996 central Australian fronts experiment. *Australian Meteorological Magazine*, *49*(3), 181–200.

Roberts, M. J., Camp, J., Seddon, J., Vidale, P. L., Hodges, K., Vanniere, B., et al. (2020). Impact of model resolution on tropical cyclone simulation using the highresmip–primavera multimodel ensemble. *Journal of Climate*, *33*(7), 2557–2583. https://doi.org/10.1175/jcli-d-19-0639.1

Roberts, M. J., Camp, J., Seddon, J., Vidale, P. L., Hodges, K., Vannière, B., et al. (2020). Projected future changes in tropical cyclones using the CMIP6 highresmip multimodel ensemble. *Geophysical Research Letters*, *47*(14), e2020GL088662. https://doi.org/10.1029/2020gl088662

Romero, R., & Emanuel, K. (2017). Climate change and hurricane-like extratropical cyclones: Projections for north Atlantic polar lows and medicanes based on CMIP5 models. *Journal of Climate*, *30*(1), 279–299. https://doi.org/10.1175/jcli-d-16-0255.1

Schreck, C. J., Knapp, K. R., & Kossin, J. P. (2014). The impact of best track discrepancies on global tropical cyclone climatologies using ibtracs. *Monthly Weather Review*, *142*(10), 3881–3899. https://doi.org/10.1175/mwr-d-14-00021.1

Schultz, D. M., & Keyser, D. (2021). Antecedents for the Shapiro–Keyser cyclone model in the Bergen school literature. *Bulletin of the American Meteorological Society*, *102*(2), E383–E398. https://doi.org/10.1175/bams-d-20-0078.1

Sherwood, S. C., Ingram, W., Tsushima, Y., Satoh, M., Roberts, M., Vidale, P. L., & O'Gorman, P. A. (2010). Relative humidity changes in a warmer climate. *Journal of Geophysical Research*, *115*(D9). https://doi.org/10.1029/2009jd012585

Shimada, U., Wada, A., Yamazaki, K., & Kitabatake, N. (2014). Roles of an upper-level cold vortex and low-level baroclinicity in the development of polar lows over the sea of Japan. *Tellus A: Dynamic Meteorology and Oceanography*, *66*(1), 24694. https://doi.org/10.3402/tellusa.v66.24694

Sikka, D. R. (2006). A study on the monsoon low pressure systems over the Indian region and their relationship with drought and excess monsoon seasonal rainfall (No. 217). *Center for Ocean-Land-Atmosphere Studies*.

Smith, E. A. (1986). The structure of the Arabian heat low. Part I: Surface energy budget. *Monthly Weather Review*, *114*(6), 1067–1083. https://doi.org/10.1175/1520-0493(1986)114<1067:tsotah>2.0.co;2

Spengler, T., Reeder, M. J., & Smith, R. K. (2005). The dynamics of heat lows in simple background flows. *Quarterly Journal of the Royal Meteorological Society*, *131*(612), 3147–3165. https://doi.org/10.1256/qj.04.177

Stansfield, A. M., & Reed, K. A. (2021). Tropical cyclone precipitation response to surface warming in aquaplanet simulations with uniform thermal forcing. *Journal of Geophysical Research: Atmospheres*, *126*(24), e2021JD035197. https://doi.org/10.1029/2021jd035197

Stansfield, A. M., Reed, K. A., Zarzycki, C. M., Ullrich, P. A., & Chavas, D. R. (2020). Assessing tropical cyclones' contribution to precipitation over the eastern United States and sensitivity to the variable-resolution domain extent. *Journal of Hydrometeorology*, *21*(7), 1425–1445. https://doi.org/10.1175/jhm-d-19-0240.1

Stoll, P. J. (2022). A global climatology of polar lows investigated for local differences and wind-shear environments. *Weather and Climate Dynamics*, *3*(2), 483–504. https://doi.org/10.5194/wcd-3-483-2022

Stoll, P. J., Graversen, R. G., Noer, G., & Hodges, K. (2018). An objective global climatology of polar lows based on reanalysis data. *Quarterly Journal of the Royal Meteorological Society*, *144*(716), 2099–2117. https://doi.org/10.1002/qj.3309

Terpstra, A., Michel, C., & Spengler, T. (2016). Forward and reverse shear environments during polar low genesis over the northeast Atlantic. *Monthly Weather Review*, *144*(4), 1341–1354. https://doi.org/10.1175/mwr-d-15-0314.1

Toomey, T., Amores, A., Marcos, M., Orfila, A., & Romero, R. (2022). Coastal hazards of tropical-like cyclones over the mediterranean sea. *Journal of Geophysical Research: Oceans*, *127*(2), e2021JC017964. https://doi.org/10.1029/2021jc017964

Tucker, D. F. (1999). The summer plateau low pressure system of Mexico. *Journal of Climate*, *12*(4), 1002–1015. https://doi.org/10.1175/1520-0442(1999)012<1002:tsplps>2.0.co;2

Ullrich, P. A. (2024). Tempestextremes v2.2.3 repository [Software]. *GitHub*. https://doi.org/10.5281/zenodo.13830377

Ullrich, P. A., & Zarzycki, C. M. (2017). Tempestextremes: A framework for scale-insensitive pointwise feature tracking on unstructured grids. *Geoscientific Model Development*, *10*(3), 1069–1090. https://doi.org/10.5194/gmd-10-1069-2017

Ullrich, P. A., Zarzycki, C. M., McClenny, E. E., Pinheiro, M. C., Stansfield, A. M., & Reed, K. A. (2021). Tempestextremes v2. 1: A community framework for feature detection, tracking and analysis in large datasets. *Geoscientific Model Development Discussions*, *2021*(8), 1–37. https://doi.org/10.5194/gmd-14-5023-2021

U.S. Navy. (1994). *Local area forecaster's handbook for naval air station Bermuda*. Naval Atlantic Meteorology Facility.

Vishnu, S., Boos, W., Ullrich, P., & O'brien, T. (2020). Assessing historical variability of south Asian monsoon lows and depressions with an optimized tracking algorithm. *Journal of Geophysical Research: Atmospheres*, *125*(15), e2020JD032977. https://doi.org/10.1029/2020jd032977

Winckler, P., Contreras-López, M., Campos-Caba, R., Beyá, J. F., & Molina, M. (2017). El temporal del 8 de agosto de 2015 en las regiones de valparaíso y coquimbo, chile central. *Latin American Journal of Aquatic Research*, *45*(4), 622–648. https://doi.org/10.3856/vol45-issue4-fulltext-1

Yamamoto, M. (2012). Rapid merger and recyclogenesis of twin extratropical cyclones leading to heavy precipitation around Japan on 9–10 October 2001. *Meteorological Applications*, *19*(1), 36–53. https://doi.org/10.1002/met.255

Yokoyama, Y., & Yamamoto, M. (2019). Influences of surface heat flux on twin cyclone structure during their explosive development over the east Asian marginal seas on 23 January 2008. *Weather and Climate Extremes*, *23*, 100198. https://doi.org/10.1016/j.wace.2019.100198

Zappa, G., Shaffrey, L., & Hodges, K. (2014). Can polar lows be objectively identified and tracked in the ecmwf operational analysis and the era-interim reanalysis? *Monthly Weather Review*, *142*(8), 2596–2608. https://doi.org/10.1175/mwr-d-14-00064.1

Zarzycki, C. M., Thatcher, D. R., & Jablonowski, C. (2017). Objective tropical cyclone extratropical transition detection in high-resolution reanalysis and climate model data. *Journal of Advances in Modeling Earth Systems*, *9*(1), 130–148. https://doi.org/10.1002/2016ms000775

Zarzycki, C. M., & Ullrich, P. A. (2017). Assessing sensitivities in algorithmic detection of tropical cyclones in climate data. *Geophysical Research Letters*, *44*(2), 1141–1149. https://doi.org/10.1002/2016gl071606

Zhang, W., Villarini, G., Scoccimarro, E., & Napolitano, F. (2021). Examining the precipitation associated with medicanes in the high-resolution era-5 reanalysis data. *International Journal of Climatology*, *41*(S1), E126–E132. https://doi.org/10.1002/joc.6669